ACS OMEGA

http://pubs.acs.org/journal/acsodf

Article

Chitosan-Based Hydrogel for the Dual Delivery of Antimicrobial Agents Against Bacterial Methicillin-Resistant *Staphylococcus aureus* Biofilm-Infected Wounds

Victoria O. Fasiku, Calvin A. Omolo,* Nikita Devnarain, Usri H. Ibrahim, Sanjeev Rambharose, Mbuso Faya, Chunderika Mocktar, Sanil D. Singh, and Thirumala Govender*

Cite This: *ACS Omega* 2021, 6, 21994−22010

Read Online

ACCESS | Metrics & More | Article Recommendations | Supporting Information

ABSTRACT: Chronic wound infections caused by antibiotic-resistant bacteria have become a global health concern. This is attributed to the biofilm-forming ability of bacteria on wound surfaces, thus enabling their persistent growth. In most cases, it leads to morbidity and in severe cases mortality. Current conventional approaches used in the treatment of biofilm wounds are proving to be ineffective due to limitations such as the inability to penetrate the biofilm matrix; hence, biofilm-related wounds remain a challenge. Therefore, there is a need for more efficient alternate therapeutic interventions. Hydrogen peroxide (HP) is a known antibacterial/antibiofilm agent; however, prolonged delivery has been challenging due to its short half-life. In this study, we developed a hydrogel for the codelivery of HP and antimicrobial peptides (Ps) against bacteria, biofilms, and wound infection associated with biofilms. The hydrogel was prepared via the Michael addition technique, and the physiochemical properties were characterized. The safety, *in vitro*, and *in vivo* antibacterial/antibiofilm activity of the hydrogel was also investigated. Results showed that the hydrogel is biosafe. A greater antibacterial effect was observed with HP-loaded hydrogels (CS-HP; hydrogel loaded with HP and CS-HP-P; hydrogel loaded with HP and peptide) when compared to HP as seen in an approximately twofold and threefold decrease in minimum inhibitory concentration values against methicillin-resistant *Staphylococcus aureus* (MRSA) bacteria, respectively. Similarly, both the HP-releasing hydrogels showed enhanced antibiofilm activity in the *in vivo* study in mice models as seen in greater wound closure and enhanced wound healing in histomorphological analysis. Interestingly, the results revealed a synergistic antibacterial/antibiofilm effect between HP and P in both *in vitro* and *in vivo* studies. The successfully prepared HP-releasing hydrogels showed the potential to combat bacterial biofilm-related infections and enhance wound healing in mice models. These results suggest that the HP-releasing hydrogels may be a superior platform for eliminating bacterial biofilms without using antibiotics in the treatment of chronic MRSA wound infections, thus improving the quality of human health.

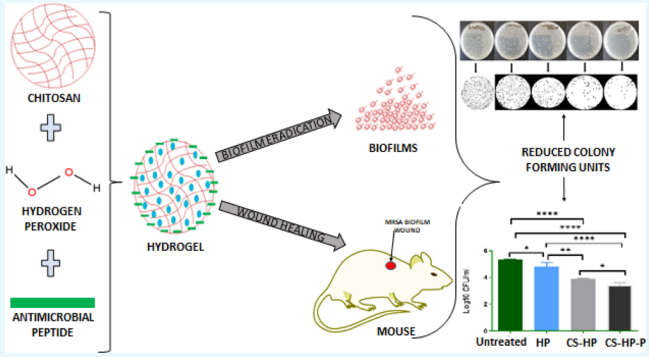

1. INTRODUCTION

Wound healing involves highly coordinated, preserved, and spatiotemporally regulated processes as well as sequential phases, viz; hemostasis, inflammation, proliferation, and remodeling.[1,2] Chronic wound infections constitute a significant burden to patients. In the United States healthcare system alone, it has been estimated that wound infections affect about 2.4−4.5 million people annually, costing approximately $20 billion.[3] Over 60% of chronic wounds have been found to be infested by biofilm communities of bacteria.[4] Biofilms are formed by a community of microorganisms embedded in a matrix of polymer, which is a mechanical barrier to immune system cells and antibiotics that enable them to survive.[5] Biofilm management has become a critical aspect of wound care. Biofilms impact wound healing by contributing to bacterial infection, inflammation, delayed healing, impaired fibroblast function, decreased angiogenesis as well as collateral damage of the surrounding tissues.[6,7] Improper management of infections associated with chronic wounds can lead to amputation and other complications such as sepsis, multiorgan failure, and even death.[8]

Over the years, several treatment modalities such as topical dressings and the use of antiseptics/disinfectants have been employed in the management of chronic/infected wounds.[9]

Received: May 15, 2021
Accepted: August 4, 2021
Published: August 19, 2021

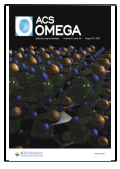

Scheme 1. Synthesis of Maleic Anhydride Grafted Chitosan (MACS)

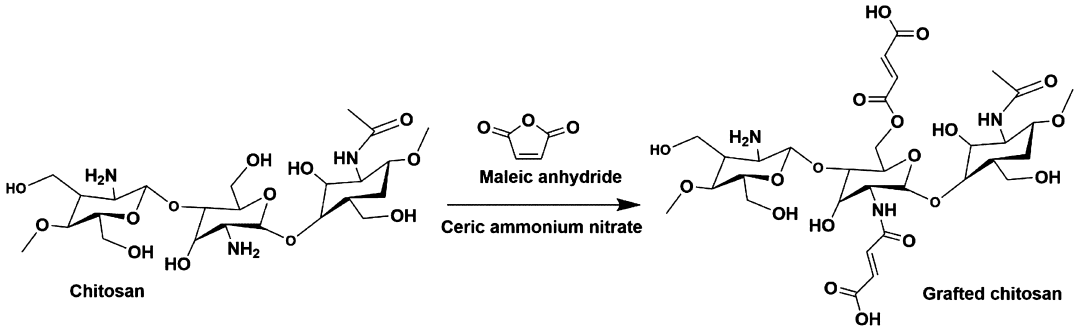

Table 1. Mutant Ps Designed by DFT

sequence	SVM score	hydrophobicity	amphipathicity	hydrophilicity	charge	PI	MW
KKKKWLLRKKC	0.95	−0.63	2.22	1.18	7.00	10.69	1459.08
RRKKWLLRKKC	0.92	−0.75	2.00	1.18	7.00	11.75	1515.10
RKKKRLLRKKC	1.11	−0.88	2.34	1.76	8.00	11.76	1457.06
RKKKWKLRKKC	0.88	−0.83	2.45	1.62	8.00	11.27	1502.10
RKKKWRLRKKC	0.96	−0.89	2.34	1.62	8.00	11.76	1530.11
RKKKWLERKKC	0.66	−0.79	2.23	1.62	6.00	10.58	1503.04
RKKKWLKRKKC	1.03	−0.83	2.45	1.62	8.00	11.27	1502.10
RKKKWLRRKKC	1.02	−0.89	2.34	1.62	8.00	11.76	1530.11

Although these conventional approaches have shown to be promising, they are limited in biofilm-wound application due to the inability to penetrate the extra polymeric matrix of the biofilms leading to a suboptimal therapeutic outcome.[10] Therefore, newer strategies and antibiofilm agents need to be explored. Recently, free radicals such as hydrogen peroxide (HP) have been discovered to have antimicrobial properties, and their antibiofilm efficacy is being investigated. Literature has shown that it is effective in reducing biofilms and enhancing wound healing.[11,12] Despite the beneficial effects, its clinical application is hampered in chronic wound infections due to its gaseous property and short half-life.[3] Furthermore, there is no consistent efficacy of HP against wound biofilms.[13] Hence, there has been increasing interest to potentiate its antibiofilm efficacy by searching for superior alternatives to improve the treatment of biofilm-related wounds.

Some strategies that can be explored to address these challenges include cocktail therapies (use of more than one antibacterial agent) and the discovery and use of biomaterials with efficient therapeutic properties.[14] The codelivery of HP with another antibacterial agent could enhance its antibiofilm properties, while the delivery system could help overcome the challenges such as the short half-life, which is associated with HP. Antimicrobial peptides (Ps) are molecules with a sequence of about 12−50 amino acid residues that are increasingly being explored for antibacterial/antibiofilm applications.[15] The major advantage of Ps over conventional antibiotics is their ability to penetrate the bacterial cell membrane and enter into intracellular targets.[16,17] Thus, various studies are investigating their antibacterial applications as codelivery agents.[16] In addition, delivery vehicles are being employed to deliver Ps to potentiate their antibacterial activity.[18] Remarkably, to date, no study has combined the delivery of Ps with HP. Therefore, the design of new Ps and codelivering them with HP using delivery vehicles such as hydrogels would be a good strategy to further enhance the antibiofilm activity of both antibacterial agents.

The use of delivery vehicles offers specific targeting to the complex normal wound healing process.[19] Hydrogels are cross-linked polymeric networks, which have pores among the polymeric chains and have been studied extensively in various biomedical applications (Scheme 1).[20] Desirable properties such as biodegradability, biocompatibility, nontoxicity, high sensitivity to physiological environments, hydrophilic nature, soft tissue-like water content, and adequate flexibility have made natural polysaccharide gels particularly excellent candidates for biomedical applications.[21] Some of the natural polymers that have been studied for antibacterial activities include chitosan. Chitosan-based hydrogels play significant roles in various stages of wound healing, which can provide a matrix for invading cells that are needed in the later phases of healing.[22] Chitosan that is derived from chitin via deacetylation is an attractive polysaccharide polymer that is biodegradable, biocompatible, and nontoxic.[23,24] Chitosan has been reported to stimulate factors for wound healing such as polymorpho-nuclear cell and fibroblast activation, cytokine production, giant cell migration, and stimulation of type IV collagen synthesis.[20] While there are reports on the synergistic effect of HP and antibiotics,[13] there are very few reports on the delivery of HP using a hydrogel.[25,26] Furthermore, there is no report on the codelivery of HP using a delivery vehicle, including hydrogels.

In this study, we, therefore, propose the codelivery of HP and Ps in a chitosan-based hydrogel. We report for the first time a novel P coloaded with HP for methicillin-resistant *Staphylococcus aureus* (MRSA) biofilm wounds. The aim of this study was to improve the wound healing and antibiofilm efficacy of HP by codelivering with a novel P (synthesized by our research group). We envisage that the incorporation of a nontoxic, novel P and HP into the hydrogel will result in the synergistic activity for antibiofilm applications. In addition, the use of the chitosan-based hydrogel as a delivery platform for the Ps and HP could provide a more efficient therapeutic

https://doi.org/10.1021/acsomega.1c02547
ACS Omega 2021, 6, 21994−22010

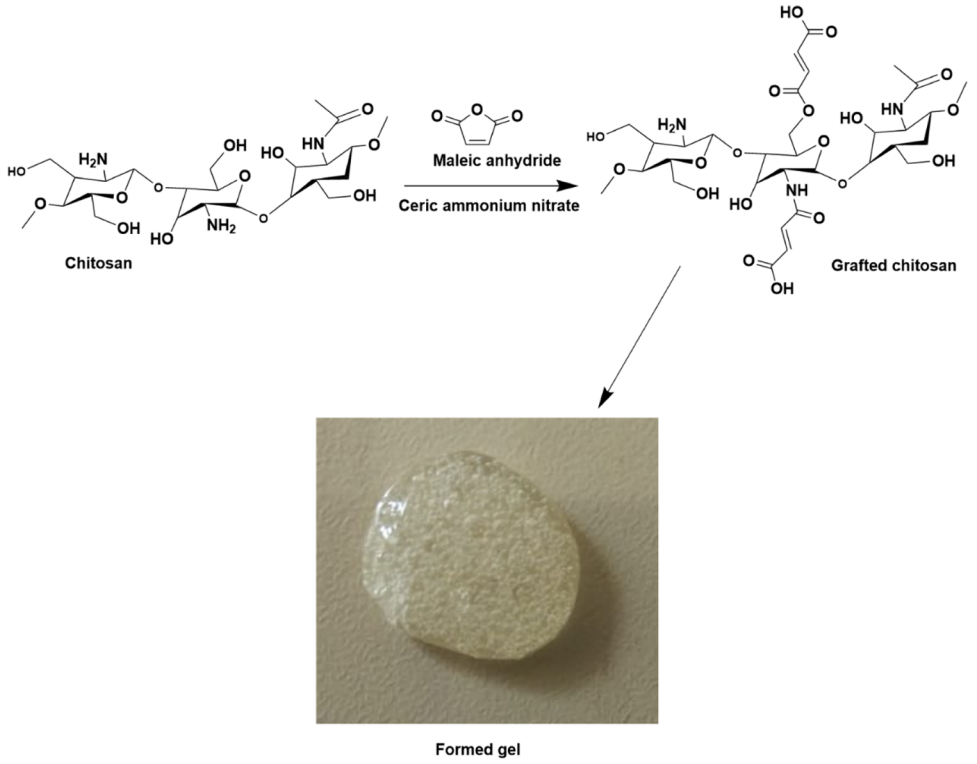

Figure 1. Preparation of the chitosan-based hydrogel.

outcome because of the ability of chitosan to accelerate wound contraction and healing.

2. RESULTS AND DISCUSSION

2.1. Design and Synthesis of the Novel Ps. All Ps were designed using the CellPPD module in the antimicrobial peptide database (APD) online tool, and the data filtering technology (DFT) was used to arrive at our desired sequences. We generated nine possible AMP mutants (Table 1). From this data filtration technology, it was observed that the frequency of LL and KK occurred frequently in the selected Ps. From the evaluation of the data, the RKKKKLLRKKC sequence was selected as the best-designed peptide for antimicrobial ability and hemolytic activity. From these computational studies, it was observed that the peptides were biocompatible and had good potential for bacterial membrane penetration.[27,28] This sequence met all the desired parameters for further evaluation. From the designed peptides, the optimum sequence was considered to be the one with the highest net positive charge (+8). Furthermore, by considering the structural motif in the data filtration process, the chosen peptide had a higher frequency of amino acids normally responsible for cell membrane permeation and biological activity. The balance of amphipathicity and hydrophobicity was also considered to be a key physicochemical consideration in selecting the desired peptide.[29] Low hydrophobicity prevents binding to the zwitterionic membranes found in mammalian cells, resulting in low toxicity and hemolysis.[30] Even though hydrophobicity is required for bacterial membrane permeabilization, higher hydrophobicity than the optimum threshold can result in the loss of biological activity and an increase in toxicity.[31] Amphipathicity allows the peptides to attack the bacterial membrane by interacting with the hydrophobic−hydrophilic character of the lipids.[32] Amphipathic structure formation also determines hemolyticity, and therefore, a low amphipathic index gives a good indication of the biological activity as well as the hemolytic potential.[33] Lastly, the data filtration technology used allowed us to examine all peptides and their respective physicochemical properties to arrive at the best possible peptide that is suitable in our formulation experiments. The synthesized and characterized peptide from China was used as received for the subsequent codelivery strategy.

2.2. Synthesis of Grafted Chitosan and Preparation of the Hydrogel. The grafted chitosan was successfully synthesized by engrafting maleic acid via redox reaction and confirmed using FTIR and NMR. The chitosan-based hydrogel (Figure 1) was prepared by reconstituting in distilled water, and the antibacterial agents (HP and P) were incorporated before further use in other experiments.

2.3. Characterization of the Hydrogel. *2.3.1. FTIR and NMR.* The chitosan grafting reaction was confirmed through FTIR and NMR characterization. The FTIR spectrum of maleic anhydride chitosan (Figure S2 in Supporting Information) shows peaks that indicate the vinyl C−H stretching and C═C stretching (maleic anhydride) at about 3100 and 1650 cm^{-1}, respectively. The broad medium peak between 2800 and 3500 cm^{-1} indicates the carboxylic OH group (O−H stretching). Also, a strong peak at around 3300 cm^{-1} represents the amide N−H stretching, while the three distinguishable peaks of ester bonds were observed at 1700, 1240, and 1050 cm^{-1}, which respectively represent stretching of C═O, C−C−O, and O−C−C bonds. These bands observed in the grated chitosan spectrum are in line with other reports of the FTIR spectrum of maleic anhydride grafted chitosan.[34] Additionally, the proton NMR spectrum of maleic anhydride chitosan (Figure S1 in Supporting Information) also confirmed the presence of maleic anhydride

https://doi.org/10.1021/acsomega.1c02547
ACS Omega 2021, 6, 21994−22010

by the presence of peaks at 6.27 and 6.76 ppm of vinyl hydrogens of the maleic anhydride.

The percentage degree grafting of chitosan was found to be 55% if the weight technique was used. The grafting percentage of chitosan by maleic anhydride was also calculated by taking into account the degree of chitosan deacetylation (DD) and integrated protons on NMR using the protons from chitosan and maleic anhydride grafts (Figures S3 and S4 of Supporting Information). The DD was calculated and found to be 0.776 using proton NMR integration, while the maleic anhydride/chitosan conjugate degree of substitution (DS) was calculated and found to be 0.487.

2.3.2. In Vitro Cytotoxicity. The cytotoxicity profile of the chitosan-based hydrogel incorporated with HP and a combination of HP/P was assessed using the MTT assay method to determine its safety for the proposed biomedical application. The cytotoxicity of the HP-releasing hydrogels was evaluated by calculating the percentage of viable mammalian cells after exposure to various concentrations (20−100 μg/mL) of the hydrogels. MCF-7, A549, and HeLa cell lines were employed in determining the biosafety of the HP-releasing hydrogels in an *in vitro* cell culture system. The results were compared to the untreated cells (negative control) and groups exposed to HP (positive control). All the cell lines showed >75% cell viability for all the concentrations of the treatments except for MCF-7, which displayed a slightly lower percentage between 70 and 74% when exposed to most concentrations of the CS-HP (hydrogel loaded with HP) hydrogel. A549 and HEK 293 cells showed percentage viability of 75.4 to 119.6% and 75.3 to 113.5%, respectively (Figure 2). There was no dose-dependent toxicity observed within the concentrations of hydrogels. These data revealed that the HP-releasing hydrogel is above the requirements for biocompatibility and toxicity regulatory requirements for biomaterials.[35,36] Thus, results from these studies revealed that CS-HP and CS-HP-P (hydrogel loaded with HP and peptide) are safe and nontoxic for biomedical applications.

2.3.3. Swelling Behavior of the Hydrogel. In order to understand the physical characteristics of the hydrogel (CS-HP-P), a swelling behavior study was performed in physiological pH at room and body temperatures (BTs) as these factors impact the swelling behavior of hydrogels.[37] The results showed a greater swelling ability of the hydrogel at BT (37 °C) when compared to RT (23 °C). The initial weight of the hydrogel (31.6 mg) increased to approximately 853 and 500 mg at 37 and 23 °C, respectively, as shown in Figure 3. The increased swelling of the hydrogel with an increase in temperature may be due to the dissociation of hydrogen bonding of amine groups in chitosan. The functional groups that may have induced thermosensitivity to the hydrogel are the primary and secondary hydroxyl groups at C-3 and C-6 positions, respectively, and the highly reactive amino group at the C-2 position. Swelling ratios ranging from approximately 3 to 27 and 2 to 15 were observed for the hydrogel at BT and RT, respectively, indicating an excellent solvent absorbency. These differences observed in the swelling capacity of the hydrogel under various temperatures are similar to those reported by Budianto and co-workers.[38] This implies that a temperature rise can lead to an increase in the swelling ability of hydrogels. Hydrogels with excellent swelling characteristics are greatly desired in several medical applications, including drug delivery. Properties such as the ability to imbibe solvent and high elasticity make these hydrogels useful in skin

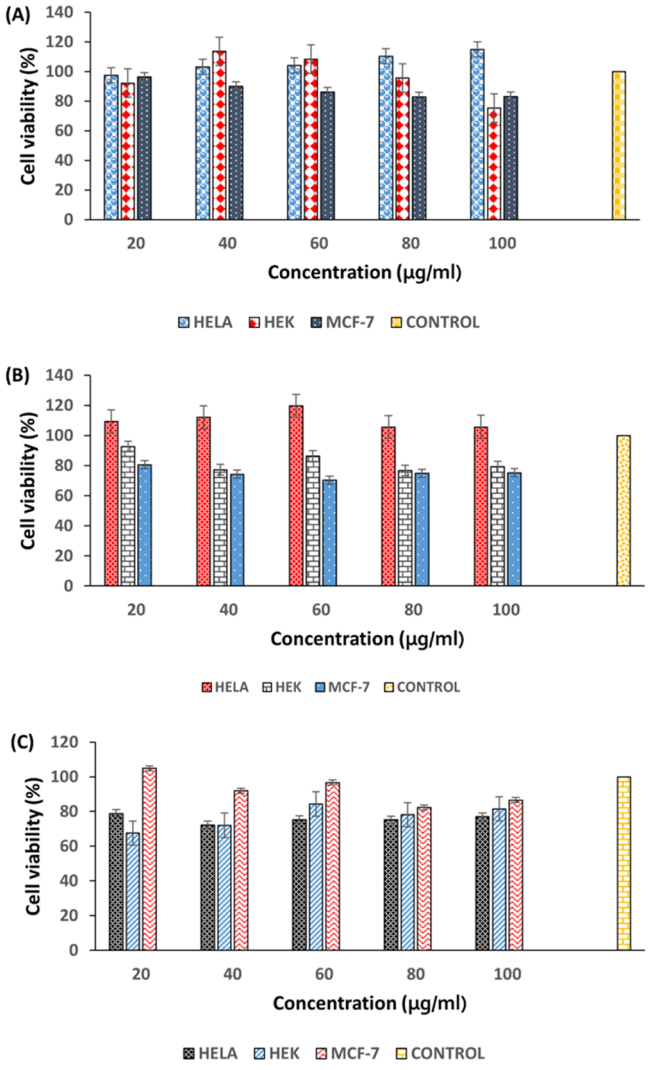

Figure 2. Percentage cell viability of different concentrations of (A) HP, (B) CS-HP, and (C) CS-HP-P on A-549, HeLa, and MCF-7 cell lines, respectively; all results are presented as mean ± SD (n = 3).

applications for wound healing.[39] Therefore, the ability of these hydrogels to swell will permit the release of the incorporated antibacterial agent (HP) through its porous structure for the intended application.

2.3.4. Rheology. Rheological assessment of hydrogels has become very critical in evaluating performance and rheological behaviors such as thixotropic behaviors. This is because it is crucial to balance the structural recovery of hydrogels after stress or strain has been applied.[40] In this study, the deformation and flow behavior of the hydrogel (CS-HP-P) were investigated. A non-Newtonian flow characteristic was displayed by the hydrogel; Figure 4 shows that the hydrogel decreased in viscosity initially due to shear thinning. The apparent viscosity of the hydrogel decreased with an increase in the shear rate. However, it was observed that the hydrogel recovered after 250 s and constant viscosity was attained. From the figure (Figure 4A), the constant shear rate applied led to the disruption of the stable hydrogel, thus becoming less viscous. Upon cessation of the steady flow of the shear rate, the hydrogel recovered its viscosity over time (Figure 4B). The non-Newtonian behavior of the hydrogel confirms its elastic and viscous nature.

https://doi.org/10.1021/acsomega.1c02547
ACS Omega 2021, 6, 21994−22010

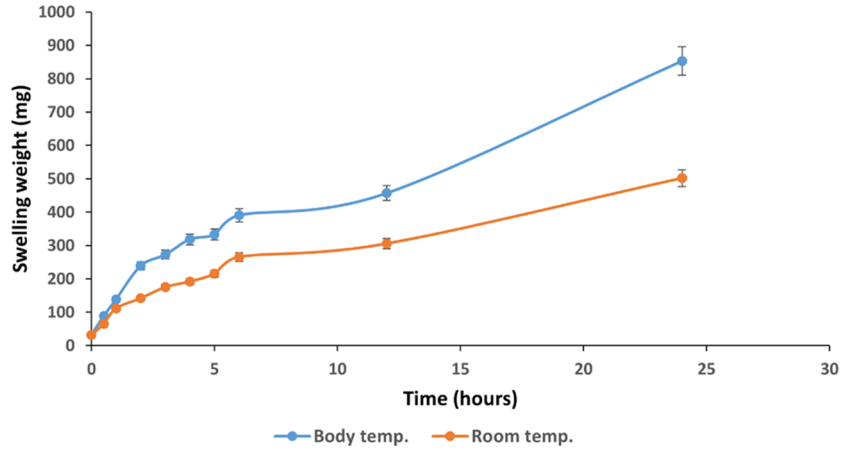

Figure 3. Hydrogel swelling capacity at BT and RT at pH 7.4 for 24 h. All results are presented as mean ± SD (n = 3).

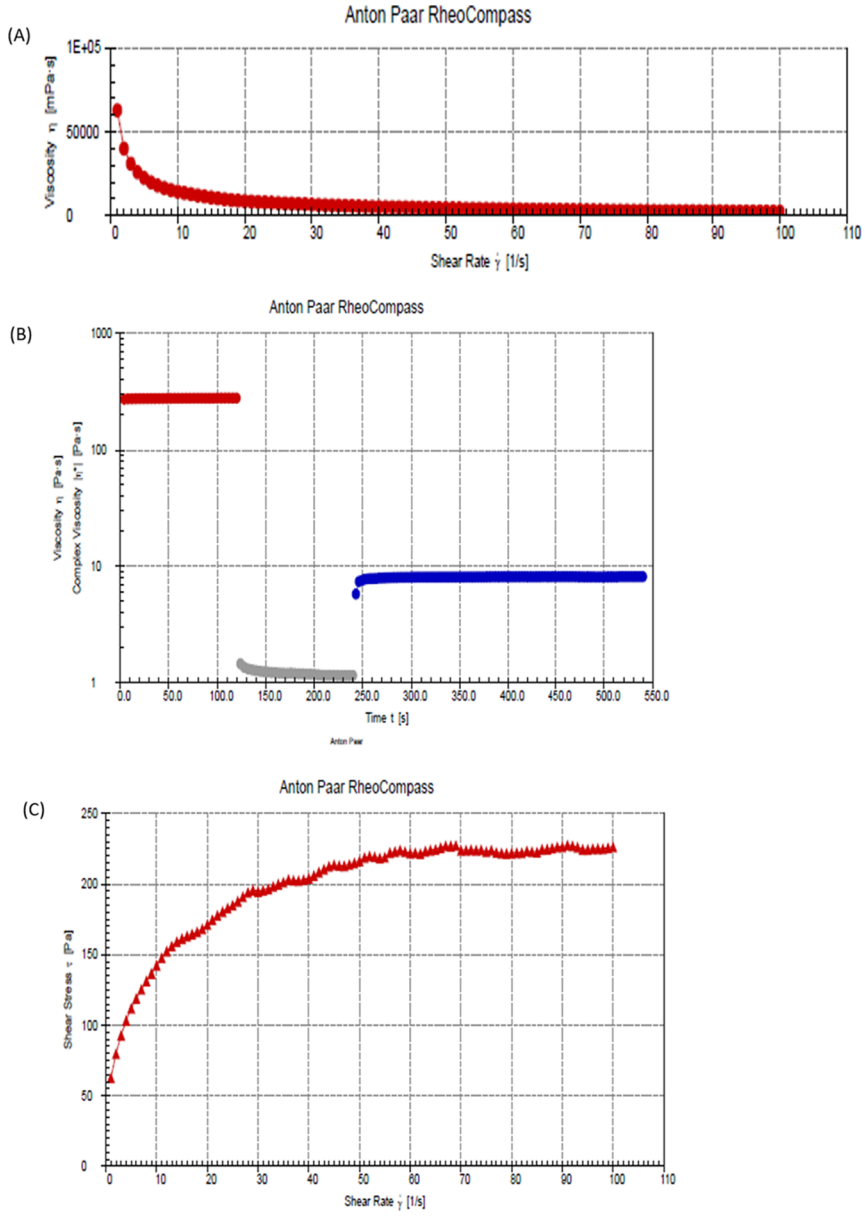

Figure 4. (A) Flow curve, (B) three-step shear recovery test, and (C) effect of shear stress on the hydrogel.

https://doi.org/10.1021/acsomega.1c02547
ACS Omega 2021, 6, 21994−22010

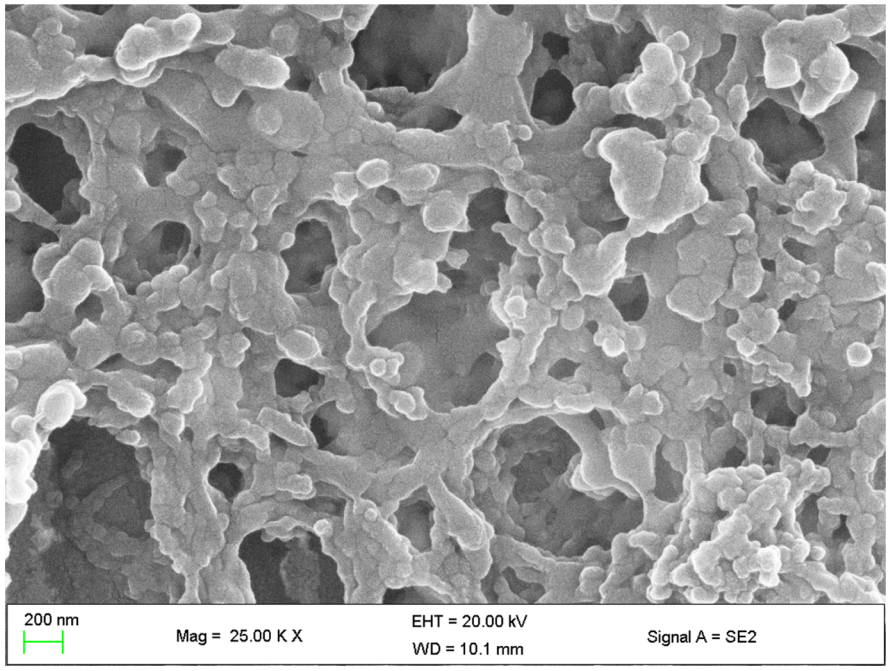

Figure 5. SEM image of the chitosan-based hydrogel.

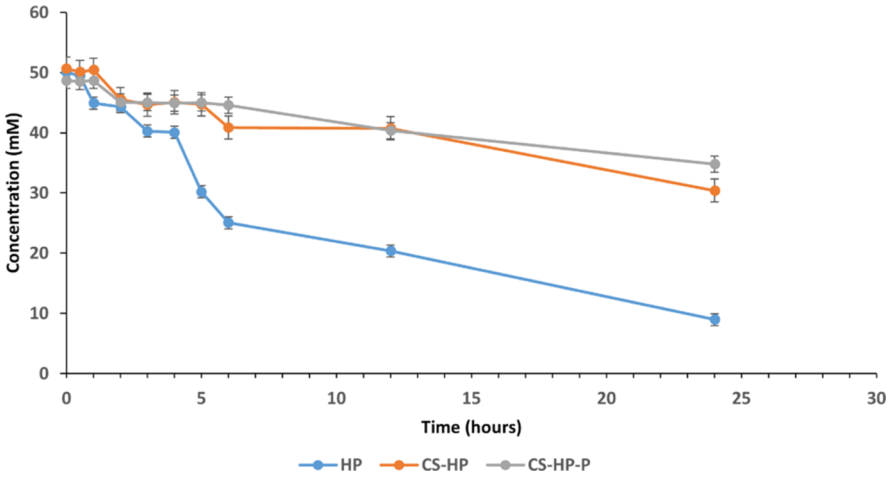

Figure 6. HP release profile from aqueous solution, CS-HP, and CS-HP-P at various times for 24 h. All results are presented as mean ± SD (n = 3).

Shear rate *versus* shear stress was already plotted (Figure 4C). From the figure, by applying the shear rate, the physical cross-links between the hydrogel temporarily break as the shear stress increased with the increase of the shear rate. However, the shear stress became constant over time. This implies that the hydrogel was no longer affected by the applied stress and was able to recover its viscous nature. This study revealed that the structural integrity of the hydrogel can be maintained intact which in turn holds the incorporated antibacterial agent within its polymeric matrix even after being subjected to stress or strain. This result of the viscosity of the hydrogel is in line with other rheological studies on the hydrogel.[41] The decline in viscosity with the increase in the shear rate further confirms the non-Newtonian behavior of the hydrogel (Figure 4A), thus suggesting that the hydrogel is suitable for the intended topical application.

2.3.5. Morphology. In several applications especially, biomedicine, evaluating the connection between the pores and the pore size of hydrogels is necessary as it determines the rate and ease of release or diffusion of the incorporated antibacterial agent.[42] The use of SEM has shown to be ideal for morphological studies; therefore, the SEM images of the hydrogel (CS-HP-P) were taken, and the images revealed the porosity of the hydrogel. Figure 5 revealed the microporous nature of the hydrogel. The captured image is similar to the previously reported chitosan-based hydrogel.[43,44] This observation supports the swelling behavior exhibited by the hydrogel as the porosity of the hydrogel will permit the release of the incorporated antibacterial agent. This indicates that hydrogels can be useful in biomedical applications that require the release of therapeutics.[45]

2.3.6. In Vitro HP Release Kinetics. The exceptional high absorptivity of crystal violet makes it ideal to be used in the photocolorimetric method to measure the concentration of HP. A change in the absorbance of the crystal violet which is a result of decoloration is closely associated with the release of HP.[46] In this study, decoloration was used to determine the release kinetics of HP. It was observed that the concentration

https://doi.org/10.1021/acsomega.1c02547
ACS Omega 2021, 6, 21994−22010

of the incorporated HP decreased with the decrease in absorbance at 245 nm at pH 7.4 at 37 °C over a period of 24 h. Figure 6 shows the progression in the decrease of the HP concentration. The initial concentration (50 mM) of HP incorporated within the polymeric matrix of the hydrogel was slowly released compared to the free HP in the buffer. A total of approximately 40, 25, and 20 mM of HP were released for HP, CS-HP, and CS-HP-P, respectively, at the end of 24 h. This revealed that the hydrogel had a slower release of HP when compared to HP in the buffer solution. This may be due to the ability of the hydrogel to prevent rapid diffusion of HP from within the polymeric matrix of the hydrogel. Notably, there was no significant difference between the concentration of HP released from the hydrogel loaded with HP alone when compared to the hydrogel coloaded with HP and peptide. This implies that P may not influence the release of HP from the hydrogel. The observation from the release study suggests that the hydrogel delivery system can be potentially employed in applications that require a slow release of the antibacterial agent for improved therapeutic outcomes.

2.3.7. Stability. In order to ensure that the hydrogel is stable, a 60-day stability study was conducted by determining the HP concentration within the hydrogel. The HP concentration decreased from 50 mM under different storage temperature conditions, as shown in Table 2. The HP concentration reduced significantly in hydrogels stored at both BT and RT, while there was no significant reduction in the HP concentration in the cold temperature (CT). This implies that the hydrogel is best stored under cold conditions.

Table 2. Concentration of HP

HP concentration (mM)	30 days			60 days		
	RT (23 °C)	BT (37 °C)	CT (8 °C)	RT (23 °C)	BT (37 °C)	CT (8 °C)
CS-HP	0	1.3	49.1	0	0	48.0
CS-HP-P	14.2	3.2	49.8	0	0	49.2

2.4. *In Vitro* Antibacterial Efficacy. *2.4.1. Minimum Inhibitory Concentration.* The *in vitro* antibacterial activity of CS, P, HP, CS-HP, and CS-HP-P was investigated using the broth dilution method. All the groups showed antibacterial activity against MRSA. Table 3 shows the minimum inhibitory concentration (MIC) values obtained after 24 h of exposing MRSA bacteria organisms to various treatments. CS-HP and CS-HP-P had approximately a 1.6- and 3.3-fold decrease, respectively, in MIC values against MRSA when compared to HP alone. Additionally, it was observed that CS-HP and CS-HP-P exhibited constant activity after 24 h, while HP did not show any activity after 24 h; this may be attributed to the unstable nature of HP.[26] The antibacterial property of P must have contributed to the enhanced antibacterial efficacy of HP when coloaded onto the hydrogel as CS-HP-P showed superior antibacterial activity than CS-HP. Ps interact with the bacterial cell membranes by neutralizing the charge and further penetrate through the bacteria to eventually cause bacterial death.[47] The effect of coloading HP and P onto the hydrogel appeared to be synergistic, and this was confirmed by determining the fractional inhibitory concentration of the test materials. The benefit of the lower MIC values obtained by loading HP onto the hydrogel includes a decrease in the frequency of administration as well as reduced side effects such as toxicity.[48] These results reveal the potential of codelivering HP and P using hydrogels against MRSA bacteria which is associated with antibiotic resistance and biofilm-related wounds.

Table 3. *In Vitro* Antibacterial Activity of Bare CS, HP, P, CS-HP, and CS-HP-P, Showing MICs against MRSA at pH 7.4

formulation	MIC (mg/mL)	
	24 h	48 h
CS	5.00	5.00
HP	0.85	0.85
P	2.50	2.50
CS-HP	0.53	0.53
CS-HP-P	0.26	0.26

2.4.2. Fractional Inhibitory Concentration. Following the recommendations by the European Committee of Antimicrobial Susceptibility Testing (EUCAST) guidelines,[49] the relationship between the antibacterial agents was determined by calculating the fractional inhibitory concentration (FIC) index values. The result showed that there was a synergistic interaction between HP and P against MRSA as seen in the FIC values. Table 4 shows that the FIC value is less than 0.5; the observed synergistic interaction may be attributed to the antibacterial mechanism of action of P, which is different from HP.[50] The observed ability of antibacterial agents to act in synergy suggests that the coloading of two or more antimicrobial agents into the same delivery vehicle can potentiate the antibacterial efficacy of the agents.[51] Therefore, challenges such as antibacterial resistance can be overcome using newer approaches like this.

Table 4. ΣFIC of HP and P against MRSA Bacteria at pH 7.4

pH 7.4	
FIC of HP	0.305
FIC of P	0.104
Σ FIC (HP + P)	0.409
interpretation	synergy

2.4.3. Time Kill Assay. The bacterial killing kinetics of CS, HP, CS-HP, and CS-HP-P was investigated using the time kill assay (TKA) technique. Figure 7 shows the bacterial killing rate when exposed to various treatments. CS and HP showed very similar bacterial killing kinetics, while CS-HP-P and CS-HP exhibited a more rapid bactericidal effect at 10 and 24 h, respectively, compared to HP. As of 24 h, HP alone did not show any bactericidal effect. This implies that the incorporation of HP into the hydrogel system can translate to a quick MRSA bacteria elimination, and a faster bacteria elimination can be achieved by incorporating Ps as seen in the hydrogel coloaded with HP and P.

2.5. Antibiofilm Study. The results from the *in vitro* antibacterial evaluation shows that CS-HP-P exhibited enhanced antibacterial activity; therefore, we investigated its antibiofilm efficacy. In order to assess the antibiofilm efficacy of the HP-releasing hydrogel, various techniques were employed. Matured MRSA biofilms were exposed to a concentration of HP-releasing hydrogels, which is within the range of treatment for biofilm eradication in the literature.[52]

https://doi.org/10.1021/acsomega.1c02547
ACS Omega 2021, 6, 21994−22010

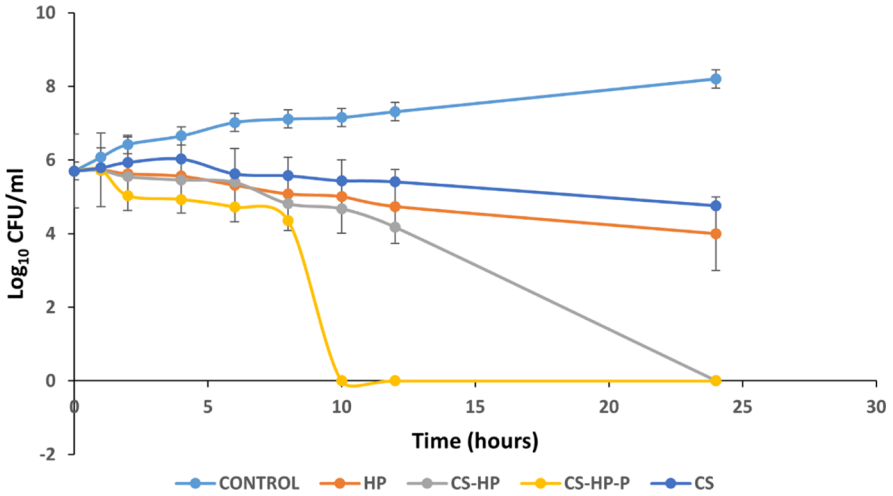

Figure 7. Killing kinetics of MRSA exposed to 5× MIC of CS, HP, CS-HP, CS-HP-P, and PBS (pH 7.4) (control). All results are presented as mean ± SD (n = 3).

2.5.1. Qualitative and Quantitative Biofilm Determination. A qualitative and quantitative technique (crystal violet staining) was used to further confirm the antibacterial/antibiofilm efficacy of CS, HP, CS-HP, and CS-HP-P against MRSA biofilms. Matured MRSA biofilms were grown in 96-well plates and were incubated with various treatment groups for 24 h. The untreated group (control) had 100% biofilm growth, while CS-, HP-, CS-HP-, and CS-HP-P-treated groups had approximately 13, 35, 62, and 75% biofilm reduction. The groups treated with the HP-releasing hydrogels were compared to the bare HP. It was observed that CS-HP had a greater biofilm eradication of approximately 27% difference when compared to HP-treated groups, while CS-HP-P-treated groups had approximately 40% difference when compared to HP-treated groups. Further comparison showed that CS-HP-P had approximately 13% biofilm reduction when compared to CS-HP. This enhanced antibiofilm efficacy exhibited by CS-HP-P may be due to the interactions between HP and P. This observation correlates with the *in vitro* antibacterial results, thus further confirming the greater efficacy of incorporating two or more antibacterial agents in hydrogels. Figure 8 shows the percentages of biofilm reduction exhibited by the various treatments and in addition, the intensity of the crystal violet stain displayed by the treatment groups. The reduction in the intensity of the stain of the hydrogel loaded with HP when compared with HP alone further confirms the enhanced antibiofilm effect of the hydrogels. CS-HP-P and CS-HP showed a reduced color intensity of the stain when compared to HP alone; however, a greater reduced intensity was observed for CS-HP-P. This observation further confirms the synergistic effect of HP and P, suggesting that CS-HP-P may be a superior alternative for the eradication of MRSA biofilms.

2.5.2. Dry Mass Quantification. Using the dry mass quantification technique, the ability of CS, HP, CS-HP, and CS-HP-P to eradicate matured biofilms formed by MRSA was investigated. After exposing the bacterial biofilms that were grown on glass slides to various treatments, the mass of the undetached biofilms was weighed. The results show that the untreated (control), CS, CS-HP, and CS-HP-P had a biofilm mass of approximately 30, 18, 12, 9, and 5 mg, respectively (Figure 9). CS-HP and CS-HP-P treatment showed reduced biomass (dry weight), which is approximately 1.3 and 2.5 times less than the HP treatment, respectively. The combination of

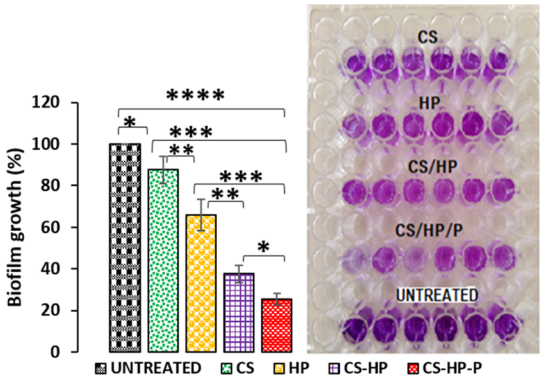

Figure 8. Percentage of biofilm growth and intensity of crystal violet stain after exposing MRSA biofilms to CS, HP, CS-HP, CS-HP-P, and untreated (control) groups. All results are presented as mean ± SD (n = 6). * denotes the significant difference of the various treatments. * denotes the significant difference of untreated *vs* CS and CS-HP *vs* CS-HP-P and ** denotes the significant difference of HP *vs* CS-HP and CS *vs* HP. *** denotes the significant difference between CS and CS-HP-P and HP *vs* CS-HP-P and **** denotes the significant difference between untreated *vs* CS-HP-P.

agents (HP and P) in the hydrogel showed a better antibiofilm activity (two times less biomass) when compared to CS-HP. This indirect method of biofilm quantification further supports other experiments in this study that showed that CS-HP-P has a greater antibiofilm activity when compared to HP and CS-HP.

2.5.3. In Vitro Biofilm Eradication. ImageJ, a Java-based imaging program, was used to automatically count the number of colony-forming units (CFUs) of matured MRSA biofilms grown on a glass slide after exposure to various treatments (HP, chitosan, CS-HP, and CS-HP-P) for 24 h. The ability of the HP-releasing hydrogel to eradicate bacterial biofilms formed on the glass slide was determined. The number of colonies counted for untreated (control), CS, CS-HP, and CS-HP-P is approximately 1000, 346, 183, 92, and 25, respectively (Figure 10). Glass slides colonized with MRSA biofilms and incubated with CS-HP-P- and CS-HP-treated groups showed enhanced biofilm eradication efficacy when compared to the HP-treated group as seen by its reduced number of colonies than the HP-treated glass slides. CS-HP-P was able to reduce

https://doi.org/10.1021/acsomega.1c02547
ACS Omega 2021, 6, 21994−22010

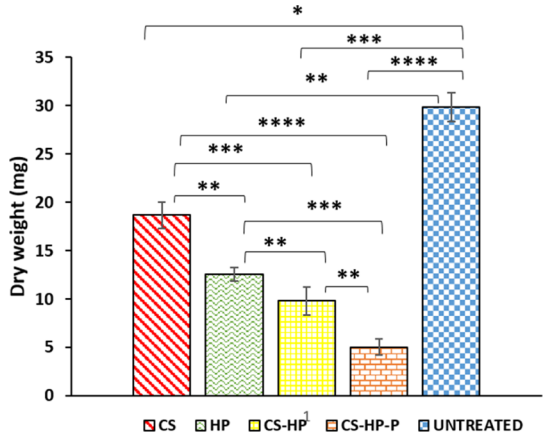

Figure 9. Dry mass of biofilms after exposing the MRSA biofilms to CS, HP, CS-HP, CS-HP-P, and untreated (control) groups. All results are presented as mean ± SD (n = 3). * denotes the significant difference of the various treatments. * denotes the significant difference of untreated *vs* CS and ** denotes the significant difference of CS-HP *vs* CS-HP-P, CS *vs* HP, HP *vs* CS-HP, and untreated *vs* HP. *** denotes the significant difference between HP and CS-HP-P, CS *vs* CS-HP, and untreated *vs* CS-HP and **** denotes the significant difference between CS *vs* CS-HP-P and untreated *vs* CS-HP-P.

the number of colonies by approximately 85%, while CS-HP reduced the number of colonies by approximately 43% when compared to HP. This result further confirms that the eradication efficacy of the hydrogel with HP and P is greatest on MRSA biofilms when compared to other treatment groups. This may also be attributed to the synergism between HP and P as observed in the other *in vitro* antibacterial/antibiofilm studies. These results suggest that the HP-releasing hydrogel prepared in this study could become a new biomaterial in eradicating bacterial biofilms that are formed on abiotic surfaces.

2.5.4. In Vivo Biofilm Wound Healing. To investigate the *in vivo* antibiofilm efficacy of the HP-releasing hydrogels (CS-HP and CS-HP-P), the hydrogels were tested against MRSA biofilm infected wounds using a mice model. The CFUs from each of the treatment groups were recovered and converted to $\log_{10}$ CFU/Ml, as shown in Figure 11A. The one-way ANOVA test showed a statistically significant (P < 0.0001) reduction in the bacterial load of recovered bacteria in all treatment groups when compared to the untreated group. The negative control (untreated), HP, CS-HP, and CS-HP-P had a bacterial load ($\log_{10}$ CFU/mL) of 5.38 ± 0.01 (244,750 CFU/mL), 4.83 ± 0.29 (78,000 CFU/mL), 3.89 ± 0.04 (7833.33 CFU/mL), and 3.40 ± 0.20 (2750 CFU/mL), respectively. These findings established that the bare HP, CS-HP, and CS-HP-P groups had a 3.13-fold (P = 0.0247), 31.24-fold (P < 0.0001), and 89.0-fold (P < 0.0001) reduction of the bacterial load when compared to the untreated group. Furthermore, the CS-HP group showed a 9.9-fold reduction of CFUs (P = 0.0011), and the CS-HP-P group showed a 28.3-fold reduction of CFUs (P = <0.0001) when compared to the HP treated group. In addition, the CS-HP-P group had a 2.8-fold reduction when compared to the CS-HP group (P = 0.0482).

The visual observation of the wound showed the presence of pus in all the groups; subsequently, no pus was observed in all the treatment groups. The wound healing progression showed that the CS-HP and CS-HP-P-treated wounds healed faster when compared to HP-treated wounds, thus further confirming their antibacterial/antibiofilm properties. At the end of the treatment period, the physical observation of the CS-HP-P-treated wounds showed approximately 90% closure, while the CS-HP-treated wounds showed approximately 80% closure; whereas, groups exposed to HP alone showed about 50% wound closure (Figure 11B). There was almost no healing and wound closure in the untreated group. In summary, the CFU results showed that wounds exposed to the HP-releasing hydrogels had lower numbers of MRSA burden when compared to wounds treated with HP alone. The enhanced antibacterial/antibiofilm efficacy of CS-HP-P observed when compared to CS-HP can be greatly attributed to the presence of the P, which potentiated the antibacterial properties of HP. This implies that Ps are promising therapeutic enhancers for existing antibacterial agents. These findings reveal hydrogels as an effective delivery system for HP and suggest the potential application of HP-releasing hydrogels in wound healing.

2.5.5. Histomorphology. The histomorphological evaluations of the wound healing process are used for evaluating the efficacy of products that influence the recovery process. Wound healing involves four sequential phases: hemostasis,

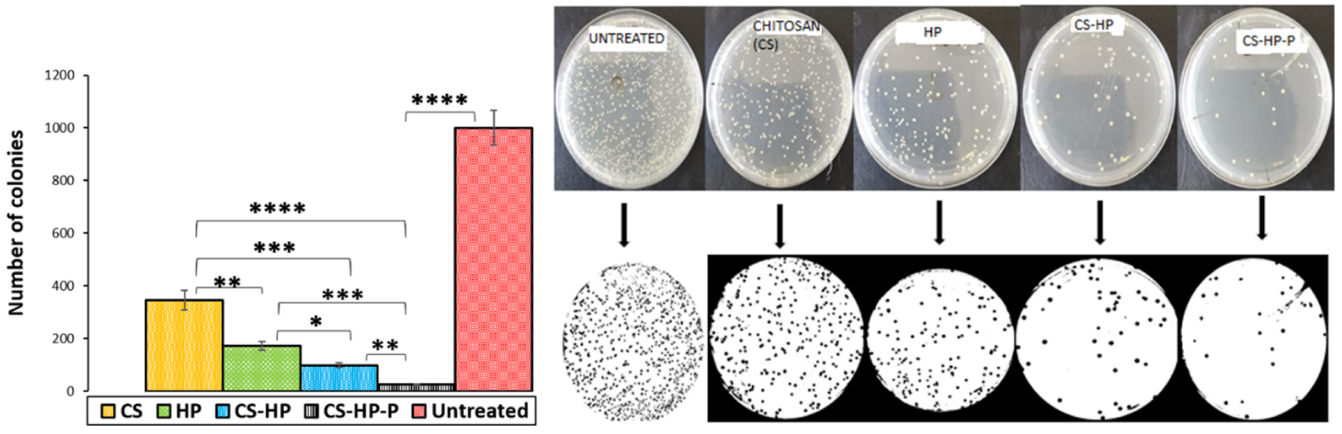

Figure 10. Number of colonies of untreated MRSA biofilms and biofilms exposed to CS, HP, CS-HP, and CS-HP-P as counted by ImageJ software. * denotes the significant difference of the various treatments. * denotes the significant difference of HP *vs* CS-HP and ** denotes the significant difference of CS-HP *vs* CS-HP-P and CS *vs* HP. *** denotes the significant difference between HP and CS-HP-P and CS *vs*-HP and **** denotes the significant difference between CS *vs* CS-HP-P and untreated *vs* CS-HP-P.

https://doi.org/10.1021/acsomega.1c02547
ACS Omega 2021, 6, 21994−22010

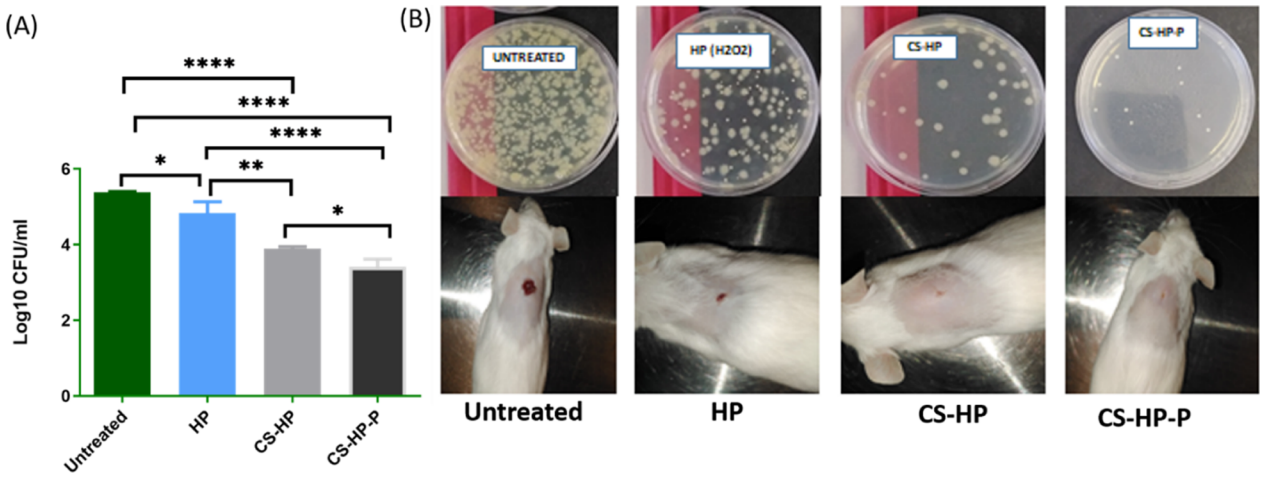

Figure 11. (A) Evaluation of MRSA burden post-treatment. Data represented as mean ± SD (n = 3). * denotes the significant difference of untreated *vs* HP and CS-HP *vs* CS-HP-P. ** denotes the significant difference of HP *vs* CS-HP. **** denotes the significant difference between untreated *vs* CS-HP and CS-HP-P and the significant difference between HP and CS-HP-P. (B) Physical observation of the wound closure and bacterial burden.

inflammation, tissue regeneration, and tissue emodeling.[53,54] In this study, tissue inflammation would have been triggered by the initial tissue injury (i.e., when creating the wound) and would have been further exacerbated by the subsequent MRSA infection to the wound. All bacteria are recognized as foreign and cause inflammation or immune responses on entry into tissues, with many components of bacteria being responsible for this response.[55,56] If the infection is confined to a local site with a small bacterial load, it will cause a controlled inflammatory response and recruit immune cells.[55,56] The greater the bacterial load within a tissue, the greater the inflammatory or immune response. Typical symptoms of acute inflammation include pain, redness, heat, and swelling.[56] Swelling can be quantified in terms of tissue thickness and is a good measure of inflammation and is useful for the quantification of skin inflammation.[57,58] Furthermore, cellular infiltration is an important aspect of skin inflammation. Neutrophils and leukocytes are the predominant type of cells that infiltrate the area. These cells play a crucial role in skin inflammation and the progression of the inflammatory reaction.[59,60] This approach has been used previously for studying the inflammatory process.[57,58,61] The skin thickness in mice in the untreated group was 4571.04 μm (Figure 12A) compared to 3236.86 μm (Figure 12B), 2002.75 μm (Figure 12C), and 1841.85 μm in mice treated with HP, CS-HP, and CS-HP-P, respectively. These findings can, therefore, be correlated with reduced swelling in these treated groups and also be correlated with the physical observations, as shown in Figure 11B. In addition, there was a considerably greater number of lymphocytes and leukocytes observed in the untreated group compared to the treated groups (Figures S3 and S4 in Supporting Information). These observations, therefore, indicate that the tissue in the HP-, CS-HP-, and CS-HP-P-treated groups [Figure 12B−D; (Figures S5C,D and S6A−D in Supporting Information)] contained comparatively less inflammation in the epidermal, dermal, and subcutaneous layers of the skin samples when compared to the untreated group [Figure 12A and (Figure S5A,B in Supporting Information)]. Although all the treated groups displayed these characteristics, the CS-HP-P-treated group displayed the greatest reduction in inflammation [Figure 12D and (S6C,D in Supporting Information)], followed by the CS-HP-treated sample [Figure 12C and (Figure S6A,B in Supporting Information)], and then the HP-treated sample [Figure 12B and (Figure S5C,D in Supporting Information)]. The histological assessments of the hematoxylin and eosin (H&E) stained sections of the untreated group [Figure 12A and (Figure S5A,B in Supporting Information)] showed a large area of ulceration, tissue inflammation with a large number of inflammatory cells, and a mild degree of vascularization in the dermal layer. The presence of these factors is indicative of incomplete healing in the untreated group and correlates with the early stages of the wound healing process in the untreated group on day 7.

Fibroblasts are responsible for the production of collagen in the skin. Collagen deposition is an important histomorphological change in the wound healing process and correlates with the remodeling phase, which is the final phase in this cascade.[53,54] Collagen is a major component of the extracellular matrix, and the wound repair process depends on the regulated production and deposition of new collagen.[62] Although H&E staining is frequently used for histomorphological analysis, this method of staining is not able to differentiate collagen deposition. This study employed PSR and CAB staining to determine the presence of collagen in the tissue sample. PSR stains collagen red and CAB stains collagen blue. The PSR and CAB staining showed an increase in collagen deposition in the treated samples (Figure 12F−H,J−L) as compared to the untreated group (Figure 12E,I). Collagen deposition is quantified by the distribution and intensity of either the blue or red color of the respective stains. The deposition of collagen in these samples correlates with the extent of tissue healing observed in H&E stained sections, that is, the samples that displayed a greater degree of wound healing in the H&E stained sections exhibited a higher deposition of collagen. The presence of collagen deposition in the treated samples correlates with later stages of the wound healing process in the treated groups (HP, CS-HP, and CS-HP-P) on day 7.

The histological assessments in this study suggest that topical application of the HP, CS-HP, and CS-HP-P treatments decreased the inflammatory response in the

https://doi.org/10.1021/acsomega.1c02547
ACS Omega 2021, 6, 21994−22010

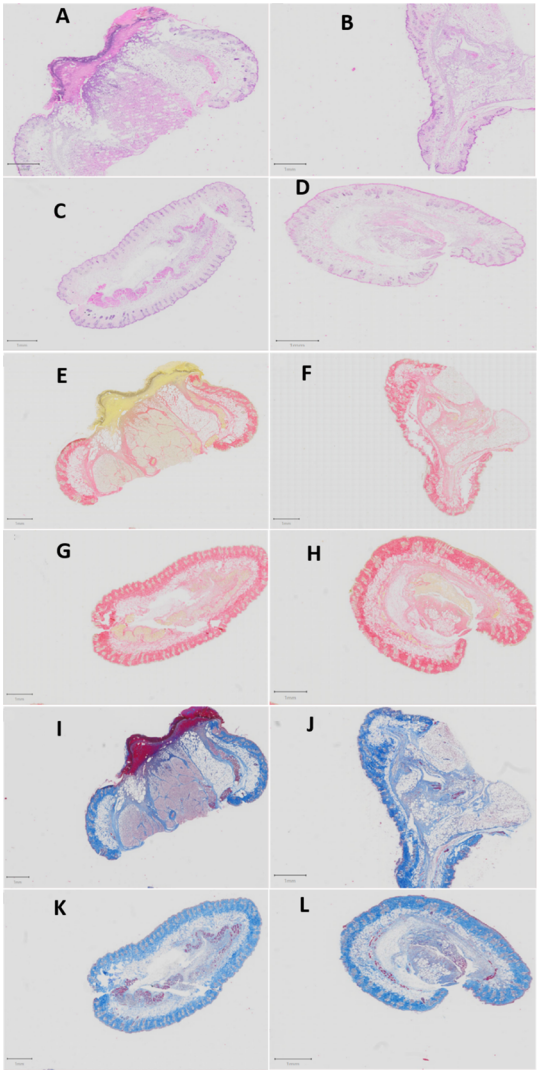

Figure 12. Photomicrographs of the untreated and treated skin sections stained with H&E, PSR, and CAB (0.5X). Untreated samples (A,E,I) stained with H&E, picrosirius red (PSR), and chromotrope aniline blue (CAB), respectively; HP samples (B,F,J) stained with H&E, PSR, and CAB, respectively; CS-HP samples (C,G,K) stained with H&E, PSR, and CAB, respectively; and CS-HP-P samples (D,H,L) stained with H&E, PSR, and CAB, respectively. Scale bar = 1 mm.

treatment groups as evidenced by the reduced swelling in the skin layers in these samples. Inflammation is one of the first responses during bacterial infection and serves as a defense mechanism against the invading organism.[63] However, a prolonged inflammatory period can extend the tissue healing process.[64] In this instance, tissue inflammation would have been triggered by the initial tissue injury (i.e., when creating the wound) and would have been further exacerbated by the subsequent MRSA infection. While infections are known to disrupt the healing cascade, the likely key element in the CS-HP-P hydrogel is the synergistic antimicrobial activity displayed by HP and P (Table 3). The results of the *in vivo* study showed that HP, CS-HP, and CS-HP-P reduced the bacterial loads significantly in the treated groups (Figure 11). This reduction in the bacterial load most likely attenuated the inflammatory response, which in turn accelerated the healing time in the HP-, CS-HP-, and CS-HP-P-treated samples. Furthermore, the reduction of inflammation in these samples directly correlates with the reduction in bacterial loads observed in these treatment groups (Figure 11). These histological findings also compare well with the physical observations shown in Figure 11B, whereby the order of wound closure was as follows: CS-HP-P > CS-HP > HP > untreated.

The H&E-, PSR-, and CAB-stained slides of tissue sections on day 7 after MRSA infection and treatment displayed that wounds treated with HP, CS-HP, and CS-HP-P showed comparatively greater tissue healing and recovery as compared to the untreated group. The extent of reduction in tissue inflammation and the presence of collagen were greater in the treatment groups when compared to the untreated samples. The results showed a trend of progressive construction of tissues surrounding the wound on day 7 for the HP-, CS-HP-, and CS-HP-P-treated groups, with the greatest progress observed in the CS-HP-P-treated group. The findings of the histomorphological studies correlate well with the evaluation of the *in vivo* MRSA burden post-treatment and the physical observations of wound closure on day 7. These findings, therefore, indicate that the CS-HP-P treatment could stimulate wound healing through the attenuation of the inflammatory response to MRSA infection and the promotion of collagen deposition that accelerates the wound repair.

3. CONCLUSIONS

In this paper, the antibiofilm and wound healing efficacy of hydrogels of natural origin for the codelivery of HP and Ps was explored. The hydrogels were prepared via the Michael addition reaction, and the antibacterial agents (HP and P) were successfully incorporated into the hydrogels. The porous structure of the hydrogels permitted a slower release of the incorporated antibacterial agent from the hydrogel matrix when compared to the release from the buffer. The hydrogel was confirmed to be biosafe/nontoxic and exhibited excellent viscosity appropriate for topical application. The *in vitro* antibacterial/antibiofilm evaluation of the HP-releasing hydrogels revealed superior antibacterial/antibiofilm efficacy against MRSA compared to HP alone as seen in lower MIC values and a reduced number of bacterial colonies. The *in vivo* wound healing studies in the MRSA biofilm-infected mice model showed a more rapid wound closure and reduced bacterial burden in groups exposed to the HP-loaded hydrogels when compared to free HP. These findings were further corroborated by the histomorphological analysis of H&E, PSR, and CAB stained sections of the tissue samples. The observed greater antibacterial/antibiofilm activity of the HP and P coloaded hydrogel demonstrated a synergetic relationship. This implies that the incorporation of the P enhanced the activity of the HP-releasing hydrogel. The results of this study suggest that combination therapy may become a better approach for targeting bacterial biofilms. Also, the HP-releasing hydrogel may serve as a new delivery system for treating chronic wound infection to achieve rapid healing, thus enhancing the quality of life.

4. MATERIALS AND METHODS

4.1. Materials. Chitosan, maleic anhydride, ceric ammonium nitrate, acetone, triethylamine, glycidylmethacrylate, tetrabutyl ammonium bromide, horseradish peroxidase (HRP), Dulbecco's phosphate-buffered saline (DPBS), iron-

https://doi.org/10.1021/acsomega.1c02547
ACS Omega 2021, 6, 21994−22010

(II) ions, crystal violet, sulfuric acid, and HP were purchased from Sigma-Aldrich (USA). P (RKKKRLLRKKC) was designed in our lab and synthesized by ChinaPeptides Co., Ltd. (China). MTT was purchased from Merck Chemicals (Germany). Mueller−Hinton Broth (MHB), nutrient broth (NB), and Mueller−Hinton Agar (MHA) used for bacterial cultures were purchased from Biolab (South Africa). MRSA Rosenbach ATCC BAA 1683 was used. Distilled water used in the study was produced in the laboratory with a Milli-Q water purification system (Millipore corp., USA). All reagents and solvents used in this study were of analytical grade.

4.2. Design of the P. The peptide was designed using DFT.[17,65] A database of highly active peptides was generated and mutants were generated using the APD online tool. From the database, the peptide length was limited to 10 amino acid residues and a charge of ≥+8. The frequency, structure type, and hydrophobicity of amino acids were considered, and a limit of hydrophobic percentage was set to range between 40 and 60%. In the design process, the filter motif was also considered, which refers to a cluster of amino acid residues that frequently occur in natural Ps. These novel Ps were further assessed on the APD online tool for novelty, charge, and hydrophobicity for their potential antimicrobial as well as biocompatibility properties. Furthermore, two online tools (*CPPpred and HemoPI*) that both use a support vector machine-based model were used to test the selected mutant peptides for their cell penetration and hemolytic activity, respectively.[66] The designed peptide was further synthesized on a large scale by ChinaPeptides Co., Ltd. (China) using the standard solid-phase peptide synthesis methodology. The peptide supplied from the company was purified using a semiprep HPLC high purity index of above 85% and their identities were further confirmed using mass spectrometry.

4.3. Synthesis of Maleic Anhydride Grafted Chitosan. The maleic anhydride grafted chitosan was synthesized by modifying a method previously reported by Hasipoglu and colleagues as well as Yucel and co-workers.[67] Briefly, 0.4 g of chitosan was dissolved in 20 mL of acetic acid solution and stirred constantly with the aid of a magnetic stirrer bar. 4 g of maleic anhydride and 1 g of ceric ammonium nitrate were added, and the mixture was left to react under continuous stirring for 3 h at 70 °C. To terminate the reaction, 20 mL of distilled water was added and the product was precipitated in acetone, filtered, and dried at a temperature of 60 °C. The degree of grafting was calculated using the change percentage of the mass of the chitosan before and after in situ gelation using equation one below[68] in weight.

$$(\%G) = \left(\frac{W_g - W_o}{W_o}\right) \times 100\% \quad (1)$$

where W_g and W_o are the weights of the grafted and pristine chitosan samples before and after in situ gelation, respectively. The degree of grafting was also determined using the proton NMR integration.

4.3.1. Incorporation of HP and P. HP was incorporated into the already prepared hydrogels by following a method reported by Lee and fellow workers.[69] Briefly, 0.04 mg of HRP was dissolved in 2 mL of DPBS and mixed with the hydrogel (55 mg of the grafted chitosan in 100 mL of water) to form solution A at a volume ratio of 1:9, while HP (50 mM) was mixed with the hydrogel to form solution B at a volume ratio of 1:9. The solutions A and B were further mixed under stirring, and the P (5 mg) was added to the mixture at RT.

4.4. Characterization of Grafted Chitosan. *4.4.1. FTIR and NMR.* In order to understand the interaction of the components of the hydrogel, a Bruker Alpha-p spectrophotometer with diamond ATR (Germany) was used by following a method previously reported by Fasiku and colleagues.[70] Maleic anhydride, chitosan, and the grafted chitosan were placed on the surface of the FTIR spectrophotometer for analysis. The analysis was carried out at a wavelength range between 4000 and 500 cm^{-1}, and scans were done 16 times at a resolution of 4 cm^{-1}. A background scan was performed to serve as a control before the sample analysis. Furthermore, NMR [^{1}H NMR (400 MHz, D_2O)] was also used to characterize the grafted chitosan in order to confirm the grafting. The DD and DS were calculated using the proton NMR integration equation (eqs 2 and 3, respectively).[71]

$$DD = 1 - \frac{A/3}{B} \quad (2)$$

where A is the proton integral that corresponds to the methyl protons of the acetylated glucosamine monomer and B is the proton integral of the carbon 2 proton of the glucosamine monomer.

$$DS = DD\frac{C/2}{B/1} \quad (3)$$

where C is the proton integral that corresponds to the vinyl protons.

4.4.2. In Vitro Cytotoxicity of the Prepared Hydrogel. The MTT assay method which has been previously reported[72] was used to investigate the *in vitro* cytotoxicity of the hydrogels. The three cell lines used in this study include human embryonic kidney (HEK-293), human breast adenocarcinoma (MCF-7), and adenocarcinomic alveolar basal epithelial cells (A-549). Briefly, all the cell lines were grown under the same conditions (temperature of 37 °C in a 5% CO_2 humidified atmosphere) until the cell lines attained 80% confluence (approximately 3.5×10^3 cells). The cells were trypsinized and seeded into 96-well plates and allowed to incubate for 24 h. The prepared hydrogel samples (with and without HP) were diluted to a final concentration of 20, 40, 60, 80, and 100 μg/mL. After 48 h, the culture medium and hydrogel samples were discarded and 100 μL of fresh medium was added to the wells. This was followed by the addition of the MTT solution (5 mg/mL in PBS). The cells were further subjected to an additional 4 h of incubation and subsequent removal of the MTT solution. By adding 100 μL of DMSO into each well, the MTT formazan was solubilized. The optical density of each well was measured using a spectrophotometer (SPECTROstar Nano, Germany) at an absorbance wavelength of 540 nm. All the experiments were performed in triplicate, and the formula below was used to calculate the percentage of viable cells:

$$\text{Cell viability } \% = \left(\frac{A540 \text{ nm treated cells}}{A540 \text{ nm untreated cells}}\right) \times 100 \quad (4)$$

4.4.3. Swelling Ability. The swelling ability of the hydrogels was determined according to the method reported by Yucel and fellow workers with slight modifications.[67] Preweighed dried hydrogel samples (31.6 mg) were inserted into a preweighed tea bag and placed in 50 mL of PBS (pH 7.4) at both BT and RT. At various time intervals (30 min for the first

https://doi.org/10.1021/acsomega.1c02547
ACS Omega 2021, 6, 21994−22010

6, 12, and 24 h), the hydrogels were blotted on a filter paper and weighed using a weighing balance. The experiment was carried out three times, and the swelling ratio and swelling capacity of the hydrogel were calculated using the equations below, respectively

$$\text{Swelling ratio} = W_t/W_0$$

SR represents the calculated swelling ratio and W_t and W_0 represent the weights of the sample at different times and dry weight, respectively.

$$\text{Swelling capacity} = \left(\frac{W_2 - W_1}{W_1}\right) \times 100\% \quad (5)$$

where W_1 represents the weight of the hydrogel before swelling and W_2 is the weight of the hydrogel post swelling.

4.4.4. Rheology. The rheological properties of the hydrogel (CS-HP-P) were determined by using an MCR 302 Rheometer (Anton Parr, Graz, Austria) with a parallel plate (PP50). The hydrogel samples were freshly prepared, placed within the plates of the rheometer, and their viscosity was measured. The apparent viscosity was calculated at 100 s^{-1} as the shear rate was applied in a linear manner from 0 to 100 s^{-1} at 25 °C.[73]

4.4.5. Morphology. The morphology of the hydrogel (CS-HP-P) was determined and imaged using SEM (ZEISS FEGSE Ultra Plus, Carl Zeiss, Oberkochen, Baden-Württemberg, Germany) at an accelerating voltage of 10 kV. The sample was prepared for analysis as per a previously reported method with slight modifications.[43] The prepared hydrogel samples were positioned on the copper grid and allowed to dry for 15 s before analyzing by SEM. A filter paper was used to remove the excess samples before capturing the image of the hydrogels.

4.4.6. In Vitro Release Kinetics of HP. The kinetics of HP that was released from the hydrogel was determined by a method reported by Alshamsi and co-workers[46] with slight modifications. The UV-spectrophotometric method was used to analyze the release kinetics of HP (50 mM) released from the hydrogels (CS-HP and CS-HP-P) using Fenton's process by decoloration reaction. Briefly, stock solution containing crystal violet solution mixed with 30 μL of 0.1 M $FeSO_4$/1 mM H_2SO_4, was prepared. The Fenton chemistry reaction was initiated by the addition of 100 μL of HP-containing hydrogels that were incubated at 37 °C to the stock solution. Aliquots were collected at various time intervals over a period of 24 h. The absorbance of the mixture was measured at a wavelength of 245 nm using a UV−visible spectrophotometer (Shimadzu UV 1601, Japan) with a temperature-controlled sample holder. The stoichiometry of the reaction between phenol and HP in the presence of Fe^{2+} in sulfuric acid medium can be expressed according to the equations below.[74]

$$Fe^{2+} + H_2O^2 \rightarrow Fe^{3+} + {}^{\bullet}OH + OH^- \quad (6)$$

$${}^{\bullet}OH + C_6H_5O\vec{H}C_6H_4(OH)_2 \quad (7)$$

4.4.7. Stability. The long-term stability of the hydrogel and the incorporated HP were evaluated for 60 days by measuring the absorbance of HP in the hydrogel (50 mM HP in CS-HP and CS-HP-P) using the UV-spectrophotometric method. The stability study was carried out under different storage conditions, viz; RT, BT, and CT as previously reported.[75]

4.5. Antibacterial Study. *4.5.1. In Vitro MIC.* The MIC study of the HP-releasing hydrogels was carried out against MRSA bacteria according to a protocol that has been reported.[76] The bacteria were cultured and grown in MHB and diluted to obtain an approximately 0.5 McFarland standard (1.5×10^8 CFU/mL). HP and HP-releasing hydrogels were serially diluted in MHB and incubated with the bacterial cultures for 24 h in a shaking incubator at 37 °C and 100 rpm. Afterward, 10 μL of the serially diluted solutions of the test samples was spotted on MHA plate and incubated for an additional 24 h. The MIC was observed at the point of no visible bacterial growth.

4.5.2. Fractional Inhibitory Concentration. The antibacterial effect of coloading HP and P within the hydrogel network was evaluated using the FIC method according to EUCAST guidelines.[49] The combined effect of HP and P was calculated based on the result of the *in vitro* antibacterial activity. The equation below was used to calculate the summation of the FICs of the individual component in order to classify the interaction of HP and peptide as either synergistic, additive, indifferent, or antagonist.[49,77,78]

ΣFIC was calculated using the following equations

$$\text{FIC of agent A} = \left(\frac{\text{MIC of agent A in combination with agent B}}{\text{MIC of agent A alone}}\right) \quad (8)$$

$$\text{FIC of agent B} = \left(\frac{\text{MIC of agent B in combination with agent A}}{\text{MIC of agent B alone}}\right) \quad (9)$$

$$\sum\text{FIC} = \text{FIC of agent A} + \text{FIC of agent B}$$

where A is HP and B is P.

The FIC index is shown in Table 5.

Table 5. FIC Index

result	synergy	additive	indifference	antagonism
index	≤0.5	>0.5 to 1	>1 to <2	≥2

4.5.3. Time Kill Assay. The bacterial killing kinetics was performed by following a previously reported method.[79,80] An overnight culture of the MRSA bacteria cultured in the NB was diluted with PBS (pH 7.4) to a concentration of 5×10^5 CFU/mL. HP, CS, and HP-releasing hydrogels, viz; CS-HP and CS-HP-P were added at 5× MIC to the bacterial MHB while sterile water was added to the bacterial broth to serve as the control. The viability of the cell was observed for 24 h; at designated times (0, 1, 2, 4, 6, 8, 10, 12, and 24 h), the samples were withdrawn and serially diluted in PBS. The samples were plated on an MHA plate and incubated for 24 h at 37 °C. After the incubation, the CFUs were counted, transformed to $\log_{10}$ values, and a graph was plotted.

4.6. Antibiofilm Study. *4.6.1. Qualitative Biofilm Determination.* A previously described method by Schuch and colleagues was employed in this experiment with slight modifications.[81] Briefly, overnight cultures of the MRSA bacteria were diluted to a concentration of the 0.5 McFarland standard, followed by the inoculation of 96-well plates with 200 μL of the diluted cultures. Matured bacterial biofilms were allowed to form by incubating the well plates at 37 °C without shaking for 7 days. Bacteria that did not form biofilms were aspirated from each well, and the wells were gently washed

https://doi.org/10.1021/acsomega.1c02547
ACS Omega 2021, 6, 21994−22010

three times with PBS. CS, HP, and HP-releasing hydrogels (CS-HP and CS-HP-P) were added at 100× MIC to each well using a sterile Pasteur pipette and incubated for 24 h. Sterile PBS was used to wash each well (three times) to remove the excess treatment. 200 μL of 100% ethanol was used to fix the biofilms before aspirating immediately and allowed to dry for 10 min. 0.01% crystal violet was used to stain the biofilms for approximately 2 min and gently aspirated from each well. The excess amount of the crystal violet stain was removed by gently washing three times with 200 μL of sterile PBS. After allowing the plate to dry for 12 h, 100 μL of 100% ethanol was added for 10 min to elute the crystal violet. The eluted stain was gently transferred to another well plate using a pipette and photographed for quantitative evaluation. The intensity of the crystal violet dye was used to determine the antibiofilm effect of the test samples. The experiment was carried out three times.

4.6.2. Dry Mass Quantification. Dry mass is a widely used maker and quick method to quantify biofilm growth, and it is usually expressed as mass per unit area or biofilm density. This experiment was performed according to a previously reported method with slight modifications.[82] MRSA biofilms were formed on standard glass microscope slides (Micro slides; VWR Scientific, Inc., West Chester, PA, USA) for 7 days. The biofilms were washed three times by gently swirling in physiological saline to detach nonadherent bacteria and treated with 100× MIC of the hydrogel samples using a sterile Pasteur pipette. The biofilms were transferred into sterile saline solution, and the adherent cells were harvested from the glass surfaces by gently scraping with a sterile spatula. The scraped biofilms were sonicated (three 10 s pulses with 5 s intervals at 50 W) using Branson Sonifier 450. Three volumes of cold ethanol were added to 5 mL of the cell suspension; the supernatant was discarded. The resulting precipitate was lyophilized and weighed using a weighing balance (Ohaus corp. Pine Brook, NJ, USA).

4.6.3. In Vitro Biofilm Eradication. The experiment was performed by counting the colonies of the bacteria using ImageJ software by following a previously reported method.[83] ImageJ has been applied to analyze biofilms in the laboratory by automatically counting the number of colonies from images. Briefly, matured biofilms of MRSA were grown on a glass slide and exposed to various treatments (HP, CS, CS-HP, and CS-HP-P) at 100× MIC for 24 h using a sterile Pasteur pipette. The glass slide was rinsed three times to remove nonadherent cells, and the biofilm on the surface of the glass slide was scraped and homogenized. The cell suspensions were plated on an MHA plate and incubated for 24 h at 37 °C. After the incubation, the colonies were photographed and converted into ImageJ pictures and automatically counted.

4.6.4. In Vivo Biofilm Wound Healing. The wound healing study was done according to the previously reported protocols[19,84] by following approval by the UKZN Biomedical Research Unit (ethical approval number AREC/042/019D). A total of 16 male BALB/c mice (7−8 weeks), divided into 4 groups, was used in the study. The mice were anesthetized using ketamine/xylazine and the region for the wound creation was shaved and disinfected. A sterile 6 mm biopsy punch was used to outline one circular pattern for the wound on the right side of the mouse's midline. Serrated forceps were used to lift the skin in the middle of the outline, and iris scissors were used to create a full-thickness wound that extends through the subcutaneous tissue. The circular piece of tissue was excised, and the wound was covered with medical tape for 24 h. After 24 h of wound excision, a membrane filter (with the preformed biofilm) was placed on the wound so that the surface with the bacterial biofilm will be in direct contact with the wound. The filter was removed from the wound, leaving behind the MRSA biofilm, and the wounds were covered with medical tape. After 24 h of MRSA biofilm inoculation, wounds were exposed to the various treatments (HP, CS-HP, and CS-HP-P), and treatments (at 100× MIC) were applied using a sterile Pasteur pipette, and the medical tape was changed daily. The progress in wound healing was observed daily and on the 7th day, the animals were humanely euthanized with isofor overdose. Prior to the study, the establishment of the biofilm was confirmed by the CFU count using the broth dilution method previously reported by Hassan and co-workers (Hassan et al., 2019). On day 7, after MRSA infection and treatment, wound tissues were excised and homogenized in sterile PBS (pH 7.4). The samples were plated on nutrient agar plates, and the bacterial colony formation unit was determined by the broth dilution technique (CFU count).

4.6.5. Histomorphological Analysis. The histomorphological analysis was carried out by excising the wounds at their largest diameter for H&E, PSR, and CAB staining. Tissue samples excised for analysis were fixed in formalin, processed, and then embedded in paraffin wax before sectioning and staining. The tissue sections were stained with H&E for general histomorphological analyses and with PSR and CAB for collagen evaluation. The stained slides were scanned using an Olympus VS120 Virtual Slide Microscope (VS120-L100-W, Olympus, Tokyo, Japan) using the ×40 objective lens. Digital slide images were then imported into QuPath, Version 0.2.3, an open-source pathology software platform for image analysis and capture.[34]

4.7. Statistical Analysis. All statistical analyses were carried out using GraphPad Prism 6 (GraphPad Software Inc., USA). All the experiments were performed in triplicate and expressed as mean ± standard deviation. In order to confirm statistical significance, the data obtained from the *in vitro* and the *in vivo* antibiofilm studies were subjected to one-way ANOVA and *t*-test. The results were considered statistically significant at a P value < 0.05 (95% significance level).

■ ASSOCIATED CONTENT

Supporting Information

The Supporting Information is available free of charge at https://pubs.acs.org/doi/10.1021/acsomega.1c02547.

H^1 NMR spectrum of maleic anhydride chitosan, FTIR images of maleic anhydride, chitosan, and grafted chitosan, swelling ratio and swelling capacity of the hydrogel at pH 7.4 at BT and RT, respectively, and histological analysis of H&E stained sections displaying cellular infiltration (PDF)

■ AUTHOR INFORMATION

Corresponding Authors

Calvin A. Omolo − *Discipline of Pharmaceutical Sciences, College of Health Sciences, University of KwaZulu-Natal, Durban 4000, South Africa; School of Pharmacy and Health Sciences, Department of Pharmaceutics, United States International University-Africa, Nairobi 00800, Kenya;* orcid.org/0000-0002-4421-3783; Email: comolo@usiu.ac.ke

Thirumala Govender − *Discipline of Pharmaceutical Sciences, College of Health Sciences, University of KwaZulu-Natal, Durban 4000, South Africa;* orcid.org/0000-0002-4968-4779; Email: govenderth@ukzn.ac.ke

Authors

Victoria O. Fasiku − *Discipline of Pharmaceutical Sciences, College of Health Sciences, University of KwaZulu-Natal, Durban 4000, South Africa*

Nikita Devnarain − *Discipline of Pharmaceutical Sciences, College of Health Sciences, University of KwaZulu-Natal, Durban 4000, South Africa*

Usri H. Ibrahim − *Discipline of Pharmaceutical Sciences, College of Health Sciences, University of KwaZulu-Natal, Durban 4000, South Africa*

Sanjeev Rambharose − *Department of Physiological Sciences, Faculty of Science, Stellenbosch University, Stellenbosch 7602, South Africa*

Mbuso Faya − *Discipline of Pharmaceutical Sciences, College of Health Sciences, University of KwaZulu-Natal, Durban 4000, South Africa*

Chunderika Mocktar − *Discipline of Pharmaceutical Sciences, College of Health Sciences, University of KwaZulu-Natal, Durban 4000, South Africa*

Sanil D. Singh − *Biomedical Research Unit, University of KwaZulu-Natal, Durban 4000, South Africa*

Complete contact information is available at: https://pubs.acs.org/10.1021/acsomega.1c02547

Notes

The authors declare no competing financial interest.

■ ACKNOWLEDGMENTS

The authors acknowledge the College of Health Sciences, University of KwaZulu-Natal (UKZN), UKZN Nanotechnology Platform, Medical Research Council, and National Research Foundation of South Africa (grant no. 106040) for their financial support and United States International University Internal grant no. 10-2879. The Biomedical Resource Unit at UKZN is also acknowledged for the technical support provided.

■ REFERENCES

(1) Eming, S. A.; Martin, P.; Tomic-Canic, M. Wound repair and regeneration: mechanisms, signaling, and translation. *Sci. Transl. Med.* **2014**, *6*, 265sr6.

(2) Pastar, I.; Stojadinovic, O.; Yin, N. C.; Ramirez, H.; Nusbaum, A. G.; Sawaya, A.; Patel, S. B.; Khalid, L.; Isseroff, R. R.; Tomic-Canic, M. Epithelialization in wound healing: a comprehensive review. *Adv. Wound Care* **2014**, *3*, 445−464.

(3) Raval, Y. S.; Mohamed, A.; Zmuda, H. M.; Patel, R.; Beyenal, H. Hydrogen-Peroxide-Generating Electrochemical Scaffold Eradicates Methicillin-Resistant Staphylococcus aureus Biofilms. *Global. Chall.* **2019**, *3*, 1800101.

(4) Mendoza, R. A.; Hsieh, J.-C.; Galiano, R. D. The Impact of Biofilm Formation on Wound Healing. In *Wound Healing-Current Perspectives*; IntechOpen, 2019.

(5) Attinger, C.; Wolcott, R. Clinically addressing biofilm in chronic wounds. *Adv. Wound Care* **2012**, *1*, 127−132.

(6) Lindley, L. E.; Stojadinovic, O.; Pastar, I.; Tomic-Canic, M. Biology and biomarkers for wound healing. *Plast. Reconstr. Surg.* **2016**, *138*, 18S.

(7) Metcalf, D.; Bowler, P. Biofilm delays wound healing: A review of the evidence. *Burns Trauma* **2013**, *1*, 5.

(8) Leaper, D.; Assadian, O.; Edmiston, C. E. Approach to chronic wound infections. *Br. J. Dermatol.* **2015**, *173*, 351−358.

(9) Negut, I.; Grumezescu, V.; Grumezescu, A. Treatment strategies for infected wounds. *Mol* **2018**, *23*, 2392.

(10) Cheng, G.; Hao, H.; Xie, S.; Wang, X.; Dai, M.; Huang, L.; Yuan, Z. Antibiotic alternatives: the substitution of antibiotics in animal husbandry? *Front. Microbiol.* **2014**, *5*, 217.

(11) Loo, A. E. K.; Halliwell, B. Effects of hydrogen peroxide in a keratinocyte-fibroblast co-culture model of wound healing. *Biochem. Biophys. Res. Commun.* **2012**, *423*, 253−258.

(12) Sultana, S. T.; Atci, E.; Babauta, J. T.; Mohamed Falghoush, A.; Snekvik, K. R.; Call, D. R.; Beyenal, H. Electrochemical scaffold generates localized, low concentration of hydrogen peroxide that inhibits bacterial pathogens and biofilms. *Sci. Rep.* **2015**, *5*, 14908.

(13) Lu, M.; Hansen, E. N. Hydrogen peroxide wound irrigation in orthopaedic surgery. *J. Bone Jt. Infect.* **2017**, *2*, 3.

(14) Alkawareek, M. Y.; Bahlool, A.; Abulateefeh, S. R.; Alkilany, A. M. Synergistic antibacterial activity of silver nanoparticles and hydrogen peroxide. *PLoS One* **2019**, *14*, No. e0220575.

(15) Sobczak, M.; Dębek, C.; Olędzka, E.; Kozłowski, R. Polymeric Systems of Antimicrobial Peptides-Strategies and Potential Applications. *Mol* **2013**, *18*, 14122−14137.

(16) Faya, M.; Kalhapure, R. S.; Kumalo, H. M.; Waddad, A. Y.; Omolo, C.; Govender, T. Conjugates and nano-delivery of antimicrobial peptides for enhancing therapeutic activity. *J. Drug Deliv. Sci. Technol.* **2018**, *44*, 153−171.

(17) Faya, M.; Hazzah, H. A.; Omolo, C. A.; Agrawal, N.; Maji, R.; Walvekar, P.; Mocktar, C.; Nkambule, B.; Rambharose, S.; Albericio, F.; de la Torre, B. G.; Govender, T. Novel formulation of antimicrobial peptides enhances antimicrobial activity against methicillin-resistant Staphylococcus aureus (MRSA). *Amino Acids* **2020**, *52*, 1439−1457.

(18) Martin-Serrano, Á.; Gómez, R.; Ortega, P.; de la Mata, F. J. Nanosystems as vehicles for the delivery of antimicrobial peptides (AMPs). *Pharmaceutics* **2019**, *11*, 448.

(19) Nurhasni, H.; Cao, J.; Choi, M.; Kim, I.; Lee, B. L.; Jung, Y.; Yoo, J.-W. Nitric oxide-releasing poly (lactic-co-glycolic acid)-polyethylenimine nanoparticles for prolonged nitric oxide release, antibacterial efficacy, and in vivo wound healing activity. *Int. J. Nanomed.* **2015**, *10*, 3065.

(20) Pal, K.; Banthia, A. K.; Majumdar, D. K. Polymeric hydrogels: characterization and biomedical applications. *Des. Monomers Polym.* **2009**, *12*, 197−220.

(21) Basso, J.; Miranda, A.; Nunes, S.; Cova, T.; Sousa, J.; Vitorino, C.; Pais, A. Hydrogel-based drug delivery nanosystems for the treatment of brain tumors. *Gels* **2018**, *4*, 62.

(22) Liu, H.; Wang, C.; Li, C.; Qin, Y.; Wang, Z.; Yang, F.; Li, Z.; Wang, J. A functional chitosan-based hydrogel as a wound dressing and drug delivery system in the treatment of wound healing. *RSC Adv.* **2018**, *8*, 7533−7549.

(23) Martínez-Martínez, M.; Rodríguez-Berna, G.; Bermejo, M.; Gonzalez-Alvarez, I.; Gonzalez-Alvarez, M.; Merino, V. Covalently crosslinked organophosphorous derivatives-chitosan hydrogel as a drug delivery system for oral administration of camptothecin. *Eur. J. Pharm. Biopharm.* **2019**, *136*, 174−183.

(24) Ahmad, N.; Ahmad, R.; Alam, M. A.; Ahmad, F. J.; Amir, M.; Pottoo, F. H.; Sarafroz, M.; Jafar, M.; Umar, K. Daunorubicin oral bioavailability enhancement by surface coated natural biodegradable macromolecule chitosan based polymeric nanoparticles. *Int. J. Biol. Macromol.* **2019**, *128*, 825−838.

(25) Lee, Y.; Son, J. Y.; Kang, J. I.; Park, K. M.; Park, K. D. Hydrogen Peroxide-Releasing Hydrogels for Enhanced Endothelial Cell Activities and Neovascularization. *ACS Appl. Mater. Interfaces* **2018**, *10*, 18372−18379.

(26) Sudur, F.; Orbey, N. Properties of hydrogen peroxide encapsulated in silica hydrogels and xerogels. *Ind. Eng. Chem. Res.* **2015**, *54*, 11251−11257.

(27) Kalafatovic, D.; Giralt, E. Cell-penetrating peptides: Design strategies beyond primary structure and amphipathicity. *Mols* **2017**, *22*, 1929.
(28) Kardani, K.; Bolhassani, A. CPPsite 2.0: An available database of experimentally validated cell-penetrating peptides predicting their secondary and tertiary structures. *J. Mol. Biol.* **2020**, *433*, 166703.
(29) Hollmann, A.; Martínez, M.; Noguera, M. E.; Augusto, M. T.; Disalvo, A.; Santos, N. C.; Semorile, L.; Maffía, P. C. Role of amphipathicity and hydrophobicity in the balance between hemolysis and peptide-membrane interactions of three related antimicrobial peptides. *Colloids Surf., B* **2016**, *141*, 528−536.
(30) Edwards, I. A.; Elliott, A. G.; Kavanagh, A. M.; Zuegg, J.; Blaskovich, M. A. T.; Cooper, M. A. Contribution of Amphipathicity and Hydrophobicity to the Antimicrobial Activity and Cytotoxicity of β-Hairpin Peptides. *ACS Infect. Dis.* **2016**, *2*, 442−450.
(31) Chen, Y.; Guarnieri, M. T.; Vasil, A. I.; Vasil, M. L.; Mant, C. T.; Hodges, R. S. Role of Peptide Hydrophobicity in the Mechanism of Action of α-Helical Antimicrobial Peptides. *Antimicrob. Agents Chemother.* **2007**, *51*, 1398−1406.
(32) Pirtskhalava, M.; Vishnepolsky, B.; Grigolava, M.; Managadze, G. Physicochemical Features and Peculiarities of Interaction of AMP with the Membrane. *Pharmaceuticals* **2021**, *14*, 471.
(33) Hansen, I. K. Ø.; Lövdahl, T.; Simonovic, D.; Hansen, K. Ø.; Andersen, A. J. C.; Devold, H.; Richard, C. S. M.; Andersen, J. H.; Strøm, M. B.; Haug, T. Antimicrobial Activity of Small Synthetic Peptides Based on the Marine Peptide Turgencin A: Prediction of Antimicrobial Peptide Sequences in a Natural Peptide and Strategy for Optimization of Potency. *Int. J. Mol. Sci.* **2020**, *21*, 5460.
(34) Bankhead, P.; Loughrey, M. B.; Fernández, J. A.; Dombrowski, Y.; McArt, D. G.; Dunne, P. D.; McQuaid, S.; Gray, R. T.; Murray, L. J.; Coleman, H. G.; James, J. A.; Salto-Tellez, M.; Hamilton, P. W. QuPath: Open source software for digital pathology image analysis. *Sci. Rep.* **2017**, *7*, 16878.
(35) Riss, T. L.; Moravec, R. A.; Niles, A. L.; Duellman, S.; Benink, H. A.; Worzella, T. J.; Minor, L. Cell viability assays. In *Assay Guidance Manual*; Eli Lilly & Company and the National Center for Advancing Translational Sciences, 2016.
(36) Hamid, R.; Rotshteyn, Y.; Rabadi, L.; Parikh, R.; Bullock, P. Comparison of alamar blue and MTT assays for high through-put screening. *Toxicol. Vitro* **2004**, *18*, 703−710.
(37) Sultana, S.; Rahaman, M. S.; Hasnine, S. M. M. Effect of Salinity on Swelling Behaviors of Superwater Absorbent Hydrogel Prepared from Carboxymethyl cellulose/Acrylamide Blends by Gamma Radiation. *Am. J. Appl. Chem.* **2018**, *2*, 20−26.
(38) Budianto, E.; Muthoharoh, S. P.; Nizardo, N. M., Effect of crosslinking agents, pH and temperature on swelling behavior of cross-linked chitosan hydrogel. *Asian J. Nat. Appl. Sci.* **2015**, *3*, 158−588.
(39) Smith, T. J.; Kennedy, J. E.; Higginbotham, C. L. The rheological and thermal characteristics of freeze-thawed hydrogels containing hydrogen peroxide for potential wound healing applications. *J. Mech. Behav. Biomed. Mater.* **2009**, *2*, 264−271.
(40) Crawford, N.; Meyer, F. *Investigating the Shear Flow and Thixotropic Behavior of Paints and Coatings*; ThermoFisher Scientific, 2014.
(41) Jyoti, B. V. S.; Baek, S. W. Rheological characterization of hydrogen peroxide gel propellant. *Int. J. Aeronaut. Space Sci.* **2014**, *15*, 199−204.
(42) Balakrishnan, B.; Banerjee, R. Biopolymer-based hydrogels for cartilage tissue engineering. *Chem. Rev.* **2011**, *111*, 4453−4474.
(43) Zahid, A. A.; Ahmed, R.; ur Rehman, S. R.; Augustine, R.; Hasan, A. In Reactive Nitrogen Species Releasing Hydrogel for Enhanced Wound Healing. *2019 41st Annual International Conference of the IEEE Engineering in Medicine and Biology Society (EMBC)*; IEEE, 2019; pp 3939−3942.
(44) Yan, S.; Wang, T.; Li, X.; Jian, Y.; Zhang, K.; Li, G.; Yin, J. Fabrication of injectable hydrogels based on poly(l-glutamic acid) and chitosan. *RSC Adv.* **2017**, *7*, 17005−17019.
(45) Ganji, F.; Vasheghani, F. S.; Vasheghani, F. E. Theoretical description of hydrogel swelling: a review. *Iran. Polym. J.* **2010**, *19*, 375−398.
(46) Alshamsi, F. A.; Albadwawi, A. S.; Alnuaimi, M. M.; Rauf, M. A.; Ashraf, S. S. Comparative efficiencies of the degradation of Crystal Violet using UV/hydrogen peroxide and Fenton's reagent. *Dyes Pigm.* **2007**, *74*, 283−287.
(47) Lei, J.; Sun, L.; Huang, S.; Zhu, C.; Li, P.; He, J.; Mackey, V.; Coy, D. H.; He, Q. The antimicrobial peptides and their potential clinical applications. *Am. J. Transl. Res.* **2019**, *11*, 3919.
(48) Li, S.; Dong, S.; Xu, W.; Tu, S.; Yan, L.; Zhao, C.; Ding, J.; Chen, X. Antibacterial hydrogels. *Adv. Sci.* **2018**, *5*, 1700527.
(49) European Committee for Antimicrobial Susceptibility Testing (EUCAST) of the European Society of Clinical Microbiology and Infectious Dieases. Terminology relating to methods for the determination of susceptibility of bacteria to antimicrobial agents. *Clin. Microbiol. Infect.* **2000**, *6*, 503−508.
(50) Dostert, M.; Belanger, C. R.; Hancock, R. E. W. Design and assessment of anti-biofilm peptides: steps toward clinical application. *J. Innate Immun.* **2019**, *11*, 193−204.
(51) Huh, A. J.; Kwon, Y. J. "Nanoantibiotics": a new paradigm for treating infectious diseases using nanomaterials in the antibiotics resistant era. *J. Controlled Release* **2011**, *156*, 128−145.
(52) Gnanadhas, D. P.; Elango, M.; Janardhanraj, S.; Srinandan, C. S.; Datey, A.; Strugnell, R. A.; Gopalan, J.; Chakravortty, D. Successful treatment of biofilm infections using shock waves combined with antibiotic therapy. *Sci. Rep.* **2015**, *5*, 17440.
(53) Elbialy, Z. I.; Atiba, A.; Abdelnaby, A.; Al-Hawary, I. I.; Elsheshtawy, A.; El-Serehy, H. A.; Abdel-Daim, M. M.; Fadl, S. E.; Assar, D. H. Collagen extract obtained from Nile tilapia (Oreochromis niloticus L.) skin accelerates wound healing in rat model via up regulating VEGF, bFGF, and α-SMA genes expression. *BMC Vet. Res.* **2020**, *16*, 352−11.
(54) Xiong, S.; Zhang, X.; Lu, P.; Wu, Y.; Wang, Q.; Sun, H.; Heng, B. C.; Bunpetch, V.; Zhang, S.; Ouyang, H. A gelatin-sulfonated silk composite scaffold based on 3D printing technology enhances skin regeneration by stimulating epidermal growth and dermal neovascularization. *Sci. Rep.* **2017**, *7*, 4288.
(55) Chaplin, D. D. Overview of the immune response. *J. Allergy Clin. Immunol.* **2010**, *125*, S3−S23.
(56) Chen, L.; Deng, H.; Cui, H.; Fang, J.; Zuo, Z.; Deng, J.; Li, Y.; Wang, X.; Zhao, L. Inflammatory responses and inflammation-associated diseases in organs. *Oncotarget* **2018**, *9*, 7204−7218.
(57) Kalhapure, R. S.; Sikwal, D. R.; Rambharose, S.; Mocktar, C.; Singh, S.; Bester, L.; Oh, J. K.; Renukuntla, J.; Govender, T. Enhancing targeted antibiotic therapy via pH responsive solid lipid nanoparticles from an acid cleavable lipid. *Nanomedicine* **2017**, *13*, 2067−2077.
(58) Cabrini, D. A.; Moresco, H. H.; Imazu, P.; Silva, C. D. d.; Pietrovski, E. F.; Mendes, D. A. G. B.; Prudente, A. d. S.; Pizzolatti, M. G.; Brighente, I. M. C.; Otuki, M. F. Analysis of the potential topical anti-inflammatory activity of Averrhoa carambola L. in mice. *J. Evidence-Based Complementary Altern. Med.* **2011**, *2011*, 908059.
(59) Sánchez, T.; Moreno, J. J. Role of leukocyte influx in tissue prostaglandin H synthase-2 overexpression induced by phorbol ester and arachidonic acid in skin. *Biochem. Pharmacol.* **1999**, *58*, 877−879.
(60) Schaerli, P.; Britschgi, M.; Keller, M.; Steiner, U. C.; Steinmann, L. S.; Moser, B.; Pichler, W. J. Characterization of human T cells that regulate neutrophilic skin inflammation. *J. Immunol.* **2004**, *173*, 2151−2158.
(61) Saito-Sasaki, N.; Sawada, Y.; Mashima, E.; Yamaguchi, T.; Ohmori, S.; Yoshioka, H.; Haruyama, S.; Okada, E.; Nakamura, M. Maresin-1 suppresses imiquimod-induced skin inflammation by regulating IL-23 receptor expression. *Sci. Rep.* **2018**, *8*, 5522−8.
(62) Upadhyay, A.; Chattopadhyay, P.; Goyary, D.; Mitra Mazumder, P.; Veer, V. Ixora coccinea enhances cutaneous wound healing by upregulating the expression of collagen and basic fibroblast growth factor. *Int. Scholarly Res. Not.* **2014**, *2014*, 751824.

https://doi.org/10.1021/acsomega.1c02547
ACS Omega 2021, 6, 21994−22010

(63) Medzhitov, R. Origin and physiological roles of inflammation. *Nature* **2008**, *454*, 428−435.
(64) Hajiaghaalipour, F.; Kanthimathi, M.; Abdulla, M. A.; Sanusi, J. The effect of Camellia sinensis on wound healing potential in an animal model. *J. Evidence-Based Complementary Altern. Med.* **2013**, *2013*, 386734.
(65) Mishra, B.; Wang, G. Ab InitioDesign of Potent Anti-MRSA Peptides Based on Database Filtering Technology. *J. Am. Chem. Soc.* **2012**, *134*, 12426−12429.
(66) Gautam, A.; Chaudhary, K.; Kumar, R.; Sharma, A.; Kapoor, P.; Tyagi, A.; Raghava, G. P. S. In silico approaches for designing highly effective cell penetrating peptides. *J. Transl. Med.* **2013**, *11*, 74.
(67) Yucel, S.; Ozdemir, Z. O.; Kesgin, C.; Terzioglu, P.; Unlu, S.; Erdogan, Y.; Pusat, K. In Swelling Behavior and Cytotoxicity of Maleic Acid Grafted Chitosan. *Proceedings of World Academy of Science, Engineering and Technology*; World Academy of Science, Engineering and Technology (WASET), 2013; p 497.
(68) Sehgal, T.; Rattan, S. Synthesis, characterization and swelling characteristics of graft copolymerized isotactic polypropylene film. *Int. J. Polym. Sci.* **2010**, *2010*, 147581.
(69) Lee, Y.; Choi, K.-H.; Park, K. M.; Lee, J.-M.; Park, B. J.; Park, K. D. In Situ Forming and H_2O_2-Releasing Hydrogels for Treatment of Drug-Resistant Bacterial Infections. *ACS Appl. Mater. Interfaces* **2017**, *9*, 16890−16899.
(70) Fasiku, V. O.; Aderibigbe, B. A.; Sadiku, E. R.; Lemmer, Y.; Owonubi, S. J.; Ray, S. S.; Mukwevho, E. Polyethylene glycol-gum acacia-based multidrug delivery system for controlled delivery of anticancer drugs. *Polym. Bull.* **2019**, *76*, 5011−5037.
(71) Pérez-Álvarez, L.; Ruiz-Rubio, L.; Vilas-Vilela, J. L. Determining the deacetylation degree of chitosan: Opportunities to learn instrumental techniques. *J. Chem. Educ.* **2018**, *95*, 1022−1028.
(72) Kalhapure, R. S.; Sikwal, D. R.; Rambharose, S.; Mocktar, C.; Singh, S.; Bester, L.; Oh, J. K.; Renukuntla, J.; Govender, T. Enhancing targeted antibiotic therapy via pH responsive solid lipid nanoparticles from an acid cleavable lipid. *Nanomedicine* **2017**, *13*, 2067−2077.
(73) Sonawane, S. J.; Kalhapure, R. S.; Jadhav, M.; Rambharose, S.; Mocktar, C.; Govender, T. Transforming linoleic acid into a nanoemulsion for enhanced activity against methicillin susceptible and resistant Staphylococcus aureus. *RSC Adv.* **2015**, *5*, 90482−90492.
(74) Shariati, R. M.; Irandoust, M.; Salarmand, N. Development of a spectrophotometric method for determination of hydrogen peroxide using response surface methodology. *Austin J. Anal. Pharm. Chem.* **2015**, *2*, 1051.
(75) Abdel-Rashid, R. S.; Helal, D. A.; Omar, M. M.; El Sisi, A. M. Nanogel loaded with surfactant based nanovesicles for enhanced ocular delivery of acetazolamide. *Int. J. Nanomed.* **2019**, *14*, 2973.
(76) Jorgensen, J. H.; Turnidge, J. D. Susceptibility test methods: dilution and disk diffusion methods. In *Manual of Clinical Microbiology*, 11th ed.; American Society of Microbiology, 2015; pp 1253−1273.
(77) Seedat, N.; Kalhapure, R. S.; Mocktar, C.; Vepuri, S.; Jadhav, M.; Soliman, M.; Govender, T. Co-encapsulation of multi-lipids and polymers enhances the performance of vancomycin in lipid-polymer hybrid nanoparticles: In vitro and in silico studies. *Mater. Sci. Eng. C* **2016**, *61*, 616−630.
(78) Maji, R.; Omolo, C. A.; Agrawal, N.; Maduray, K.; Hassan, D.; Mokhtar, C.; Mackhraj, I.; Govender, T. pH-Responsive Lipid-Dendrimer Hybrid Nanoparticles: An Approach To Target and Eliminate Intracellular Pathogens. *Mol. Pharm.* **2019**, *16*, 4594−4609.
(79) Mohamed, M. F.; Hamed, M. I.; Panitch, A.; Seleem, M. N. Targeting methicillin-resistant Staphylococcus aureus with short salt-resistant synthetic peptides. *Antimicrob. Agents Chemother.* **2014**, *58*, 4113−4122.
(80) Omolo, C. A.; Kalhapure, R. S.; Agrawal, N.; Jadhav, M.; Rambharose, S.; Mocktar, C.; Govender, T. A hybrid of mPEG-b-PCL and G1-PEA dendrimer for enhancing delivery of antibiotics. *J. Controlled Release* **2018**, *290*, 112−128.
(81) Schuch, R.; Khan, B. K.; Raz, A.; Rotolo, J. A.; Wittekind, M. Bacteriophage lysin CF-301, a potent antistaphylococcal biofilm agent. *Antimicrob. Agents Chemother.* **2017**, *61*, e02666−16.
(82) Koo, H.; Hayacibara, M.; Schobel, B.; Cury, J.; Rosalen, P.; Park, Y.; Vacca-Smith, A.; Bowen, W. Inhibition of Streptococcus mutans biofilm accumulation and polysaccharide production by apigenin and tt-farnesol. *J. Antimicrob. Chemother.* **2003**, *52*, 782−789.
(83) Schulze, K.; López, D. A.; Tillich, U. M.; Frohme, M. A simple viability analysis for unicellular cyanobacteria using a new autofluorescence assay, automated microscopy, and ImageJ. *BMC Biotechnol.* **2011**, *11*, 118−8.
(84) Kim, J. O.; Noh, J.-K.; Thapa, R. K.; Hasan, N.; Choi, M.; Kim, J. H.; Lee, J.-H.; Ku, S. K.; Yoo, J.-W. Nitric oxide-releasing chitosan film for enhanced antibacterial and in vivo wound-healing efficacy. *Int. J. Biol. Macromol.* **2015**, *79*, 217−225.

https://doi.org/10.1021/acsomega.1c02547
ACS Omega 2021, 6, 21994−22010